FINAL REPORT

Rheological Characterization and Biological and Mass Transfer Kinetics of Cellulase-Producing *T. reesei* Viscous Suspensions

Mark R. Marten, Svetlana Velkovska, Saad A. Khan, and David F. Ollis, Chemical Enginering Department, NCSU, Raleigh, NC 27695-7905

Sponsor: National Renewable Energy Laboratory
April, 1995

Contents

List of Figures

1 Introduction

In the biomass-to-ethanol conversion process, cellulase enzymes are used to convert cellulosic biomass to fermenatable–sugar feedstock, for conversion to ethanol. The cellulase enzymes used in the hydrolysis process are most often produced in aerobic, fungal cultures, in which mycelial cell growth transforms the broth from a Newtonian mixture into a non-Newtonian suspension with time varying rheological properties and high apparent viscosities. High broth viscosity has the potential to reduce mass and momentum transfer capacity and thus can detrimentally effect cell growth and enzyme production. To improve cell growth and enzyme production, aeration and agitation strategies must be formulated that ensure adequate oxygen and nutrient transfer to the mycelia, without adverse effects on cellulase–activity production. These aims require that both the biological and physical kinetics of these fungal cultures be better understood. Biological kinetics involve cell growth, substrate (nutrient) consumption, and product (cellulase) formation rates, while physical kinetics involve the evolution of rheological properties and their effect on oxygen supply and mixing in the fermentor. Our ultimate goal is a complete biological and physical kinetic description of cellulase producing fungal fermentations, which could lead to strategic improvements in cellulase production reactors.

This goal may alternatively be stated in three parts:

1. Physical Kinetics: establish which simple fluid constitutive model fits the steady shear rheology data for shear-stress vs shear-rate, for various cultivation times and mycelial quality.

2. Biological Kinetics: develop a fundamental model for the relationship between biomass growth, cellulase-enzyme product formation, and substrate-cellulase conversion.

3. Physical/Biological Kinetics Interaction: develop understanding, through correlations, of fermentation regimes of either oxygen limitation or oxygen sufficiency, and of agitation sufficiency or insufficiency for fluid mixing.

To address these three challenges, we performed numerous fermentations with the mycelial fungus *Trichoderma reesei* RUT-C30, in a 16 L fermentor with Solka Floc 200FCC used as model cellulose nutrient. Chapter one of this report describes the evolution of broth rheology, and the resulting Casson model parameters which were found to fit the shear-stress shear-rate data for all degrees of cellulose conversion (0 – 100%), and oxygen mass transfer characteristics, for several different fermentor impeller speeds. We found that a low fermentor impeller speed led to oxygen limited cell growth and to reduced cellulase activity production. To eliminate this circumstance, pure oxygen was added as needed to the air sparge stream in lower agitator-speed runs, allowing us to determine the intrinsic biological kinetics of this fungal strain. Chapter two details all biological kinetic data acquired, and develops the

biological kinetic model, which describes non-oxygen-limited cell growth, cellulose-nutrient consumption, and cellulase-activity production. The resultant model describes fermentations from 0 – 100% cellulose conversion, and is the first to include all of the four phenomena listed below which are established to be important in *T. reesei* biological kinetics:

1. structured biomass, consisting of primary and secondary mycelia.
2. enzyme (cellulase) production by secondary mycelia only.
3. cellulase partitioning between solution (free enzyme) and cellulose (adsorbed enzyme).
4. substrate cellulose reactivity which declines with degree of cellulose conversion.

2 Rheological, Mass Transfer, and Mixing Characterization of Cellulase Producing *Trichoderma reesei* Suspensions (A paper submitted to *Biotechnology Progress*)

2.1 Abstract

Steady and dynamic shear measurements are utilized to characterize the rheological behavior of *Trichoderma reesei* RUT-C30 fungal suspensions during batch growth on xylose (soluble substrate) or cellulose (particulate solid substrate) at three different fermentor impeller speeds (250, 400 and 550 rpm). Biomass concentrations versus time were unimodal on xylose and bimodal on cellulose. This behavior is consistent with relatively rapid, early growth on easily metabolized growth medium components (yeast extract), followed by a second, slower growth phase due to hydrolysis of recalcitrant cellulose by increasing cellulase concentrations. Critical dissolved oxygen (DO) concentration for *T. reesei* growth on cellulose was found to be 0.073 mmol/L. The DO was kept above this level by supplementing air feed with pure oxygen, implying that mass transfer limitations were not the cause of bimodal cell growth. Steady shear rheological data showed shear thinning behavior and a yield stress for all broth samples regardless of substrate. Casson and Herschel-Bulkley constitutive equations fit steady shear data well. Dynamic shear measurements on broth suspensions indicated a "gel-like" behavior at low strains, with microstructural breakdown at larger displacements. Time variations of the Casson model parameters (yield stress and Casson viscosity) and dynamic moduli (elastic and viscous modulus) strongly followed biomass profiles: a single maximum in all rheological variables resulted when cells were grown on xylose, or on cellulose at impeller speeds of 400 or 550 rpm, and dual maxima were observed for cellulose-grown cells at 250 rpm.

2.2 Symbols Used in Chapter 2

A	constant defined in Equation 13
C^*	dissolved oxygen concentration in equilibrium with the exit gas, mmol O_2 L^{-1}
C_l	dissolved oxygen concentration, mmol O_2 L^{-1}
c	geometric vane constant, dimensionless
D_c	yield stress cavern diameter, cm
D_i	impeller diameter, cm
G'	elastic (storage) modulus, dyn cm^{-2}
G"	viscous (loss), dyn cm^{-2}
H_c	yield stress cavern height, cm
K	power law consistency, dyn s^n cm^{-2}
K_c	Casson model viscosity, $poise^{\frac{1}{2}}$
K_{HB}	Herschel Bulkley model consistency, dyn $s^{n_{HB}}$ cm^{-2}
k	geometric vane constant, dimensionless
$k_l a$	mass transfer conductance, hr^{-1}
M	impeller torque, dyn cm
N	impeller rotational speed, s^{-1}
N_A	volumetric oxygen transfer rate, mmol $O_2 L^{-1} hr^{-1}$
N_P	power number, dimensionless
N_{Pot}	turbulent power number, dimensionless
N_{Re}	Reynolds number, dimensionless
N_{Re_y}	yield stress Reynolds number, dimensionless
N_w	impeller speed at which the cavernreaches the vessel wall, s^{-1}
n	power law index, dimensionless
n_{HB}	Herschel Bulkley model index, dimensionless
P	power input, dyn cm s^{-1}
T	tank diameter, cm
t	time, s
$\dot{\gamma}$	shear rate, s^{-1}
$\dot{\gamma}_{avg}$	average shear rate, s^{-1}
η	apparent viscosity, poise
ρ_l	liquid density, g cm^{-3}
τ	shear stress, dyn cm^{-2}
τ_{avg}	average shear stress, dyn cm^{-2}
τ_y	yield stress, dyn cm^{-2}
$\tau_{y_{HB}}$	Herschel Bulkley model yield stress, dyn cm^{-2}
τ_{yx}	shear stress, dyn cm^{-2}
ω	frequancey, rad s^{-1}

2.3 Introduction

Renewable resources will play a significant role in the world's future chemical and energy needs. In line with this fact, the U.S. Department of Energy has indicated that an important mid-term priority is the efficient conversion of cellulosic biomass to a sugar-containing feed stock, suitable for microbial conversion to fuel-ethanol (Bozell and Landucci, 1993). Acid hydrolysis, one of the methods often employed for this process, subjects cellulose to a severe environment leading to formation of undesirable waste streams and degradation byproducts. (Mohagheghi et al., 1988). These byproducts must then be removed from the product sugars prior to use in ethanol fermentations. In contrast, enzymatic hydrolysis yields a sugar-rich feed stock, free of harmful byproducts, which is readily utilized by ethanol-producing microorganisms.

The cellulase enzymes used in the hydrolysis process are often produced in aerobic, fungal cultures of *Trichoderma reesei*, where mycelial cell growth and propagation transforms the broth from a Newtonian mixture into a non-Newtonian suspension with time varying rheological properties and high apparent viscosities. High broth viscosity has the potential to reduce mass and momentum transfer capacity and thus can detrimentally effect cell growth and enzyme production. To improve cell growth and enzyme production, aeration and agitation strategies must be formulated that ensure adequate oxygen and nutrient transfer to the mycelia, without adverse effects on cellulase–activity production. These aims require that both the biological and physical kinetics of these fungal cultures be better understood. Biological kinetics involve cell growth, substrate (nutrient) consumption, and product (cellulase) formation rates, while physical kinetics involve the evolution of rheological properties and their effect on mass and momentum transport in the fermentor. Our ultimate goal is a complete biological and physical kinetic description of cellulase producing fungal fermentations, which could lead to strategic improvements in cellulase production reactors.

As an initial step toward this goal, we report here the rheological behavior of *Trichoderma reesei* RUT-C30 fungal fermentations grown on particulate solid substrate. Little is known about the rheological behavior of this industrially important strain and, to our knowledge, no one has yet investigated the rheological behavior of a fungal suspension grown on a particulate solid. We explore how oxygen limitations affected both biological kinetics and bubble-free broth rheology. We quantitate rheological behavior with both steady and dynamic shear techniques, and determine which rheological model best represents the steady shear data. This information is then used to establish how broth rheology changed over the course of batch fermentations at three different impeller speeds (250, 400, 550 rpm). Preliminary rheological results were reported previously (Marten et al., 1994), the full study appears here. A biological kinetic model, which is presented elsewhere (Velkovska et al., 1995), is constructed for cell growth, substrate consumption and product expression.

We conducted both steady and dynamic shear rheological measurements (off-line), in a specially designed vane-and-cup geometry. We chose this configuration because more

conventional rheometer geometries (e.g. cone and plate, concentric cylinders) can lead to large measurement errors due to the suspension nature of the broth (Charles, 1978; Metz et al., 1979). The vane-and-cup system was first calibrated using fluids of known rheological character. Then, *T reesei* cells were grown on particulate-solid cellulose suspensions under several shear and aeration conditions. Samples were taken at various times during fermentations, and portions were prepared for later analysis of cell mass, residual substrate, and cellulase activity. The remainder of the sample was used for both steady and dynamic shear rheological experiments.

Many researchers have studied the rheological behavior of fungal suspensions under steady shear conditions (Metz et al., 1979; Reuss et al., 1982; Oolman and Blanch, 1986; Kemblowski and Kristiansen, 1986; Allen and Robinson, 1990). During these experiments, in which the viscosity (η, poise) of the sample is measured as a function of shear rate ($\dot{\gamma}$, s^{-1}), the behavior of fungal cell suspensions is invariably pseudoplastic or shear thinning (Metz et al., 1979; Reuss et al., 1982), i.e. the viscosity decreases with increasing shear rate. Among the different constitutive expressions used to model this behavior, the two most common (Metz et al., 1979) are the power law model given by equation 1:

$$\tau = K(\dot{\gamma})^n \tag{1}$$

where K (dyn·s^n/cm^2) and n are the power law consistency and index respectively, and the Casson model given by equation 2:

$$(\tau)^{\frac{1}{2}} = (\tau_y)^{\frac{1}{2}} + K_c(\dot{\gamma})^{\frac{1}{2}} \tag{2}$$

where τ_y (dyn/cm^2) is the Casson yield stress and K_c (poise$^{\frac{1}{2}}$) is the Casson viscosity. Another constitutive expression, used much less frequently, is the Herschel-Bulkley model given by equation 3:

$$\tau = \tau_{y_{HB}} + K_{HB}\dot{\gamma}^{n_{HB}} \tag{3}$$

where $\tau_{y_{HB}}$ (dyn/cm^2), K_{HB} (dyn·s$^{n_{HB}}$/cm^2), and n_{HB} are the Herschel-Bulkley yield stress, consistency, and index respectively. Reuss et al. (Reuss et al., 1982) speculated that any of these different shear thinning models could adequately represent steady shear rheological behavior in the limited shear rate ranges over which suspension measurements are typically taken. Reuss therefore suggested that for simplicity, the power law model be used. The power law model however, does not incorporate a yield stress, and *T. reesei* grown on particulate cellulose has been observed to produce uneven mixing and stagnant regions in the fermentation vessel (Mohagheghi, 1993) indicative of a fluid yield stress. Therefore, in our study we examined which of these three simple fluid models best correlated steady shear behavior for these fungal suspensions.

To characterize microstructure in our fermentation-broth suspensions, we used dynamic rheological (oscillatory strain) measurements. This technique involves imposing a sinusoidaly varying deformation on a fluid sample, and measuring both the resulting torque

and the phase angle between the imposed shear strain and the torque. Effective probing of material microstructure without disrupting it is possible by applying a small amplitude strain to the sample (Aranguren et al., 1992; Khan and Zoeller, 1993). Alternatively, application of large strains enables determination of the sensitivity of the microstructure to shear (Khan et al., 1994; Kilpatrick et al., 1994). For polymers, a large body of literature exists which relates dynamic rheological parameters to polymer molecular structure (Ferry, 1980; Bird et al., 1987; Graessley, 1993). In contrast, little has been published on the viscoelastic properties of fungal broths (Oolman et al., 1987; Chmiel et al., 1990). We have used oscillatory strain rheological measurements to determine the dynamic moduli of the mixed suspensions (mycelial cell mass and solid cellulose particles) in our fermentation broths, and correlated them with steady shear and biomass behavior.

2.4 Materials and Methods

Strain. For storage, *Trichoderma reesei* RUT-C30 (ATCC 56765) cultures were grown on potato dextrose agar at 28 °C. After sporulation, *T. reesei* spores were resuspended in 10% glycerol solution and stored in sterile 1.5 mL microfuge tubes at -70 °C.

Medium and Inoculum. The inoculum and production media were prepared as described previously (Mohagheghi et al., 1988) with minor modifications (Mohagheghi, 1993). Frozen stock culture was used to inoculate a 250 mL baffled flask containing 50 mL growth medium A (0.4 g/L $CaCl_2 \cdot 2H_2O$, 0.3 g/L $MgSO_4 \cdot 7H_2O$, 2.0 g/L KH_2PO_4, 1.7 g/L $(NH_4)_2SO_4$, 10 g/L yeast extract (Difco), 5.0 mg/L $FeSO_4 \cdot 7H_2O$, 1.6 mg/L $MnSO_4 \cdot H_2O$, 1.4 mg/L $ZnCO_4 \cdot 7H_2O$, 3.7 mg/L $CoCl_2 \cdot 6H_2O$) with 10 g/L glucose. After 2.5 days, the contents of the pre-inoculum flask were used to inoculate a 2.8 L baffled, Fernbach flask containing 1000 mL of medium A with 10 g/L cellulose (Solka Floc 200FCC, 35μm nominal fiber length, Fiber Sales and Development Corp., Urbana, OH). All flasks were incubated at 28 ^{0}C on an oscillating shaker at 225 rpm.

Fermentation Conditions. Fermentations were carried out in a 16 L, in-place sterilizable fermentor (Microgen SF116, New Brunswick Scientific, Edison, NJ) with a 10 L working volume. The fermentor was filled with 500 g Cellulose, 8.0 g $CaCl_2 \cdot 2H_2O$, 6.0 g $MgSO_4 \cdot 7H_2O$, 37.0 g KH_2PO_4, 66.0 g $(NH_4)_2SO_4$, 100 g yeast extract, 2.0 mL Tween 80, 50 mg $FeSO_4 \cdot 7H_2O$, 16 mg $MnSO_4 \cdot H_2O$, 14 mg $ZnCO_4 \cdot 7H_2O$, 37 mg $CoCl_2 \cdot 6H_2O$, brought to a volume of 9.0 L with distilled water, sterilized, and inoculated with 1000 mL of broth from the Fernbach inoculum flask. The culture was maintained at 28 °C, 250 rpm, and was sparged with air between 0.2 and 1.0 vol/vol/min. Dissolved oxygen concentration was maintained above 20% by supplementing air with oxygen, unless otherwise noted. Fermentor–headspace pressure was controlled at 2 psig. A pH of 4.8 was maintained by addition of NH_4OH (3M) or H_3PO_4 (3M). Foaming was prevented by automatic addition of Antifoam 289 (Sigma Chemical Co.). To prevent bacterial contamination, antibiotics penicillin and streptomycin

were added to the fermentor (500 mg/L final concentration of each).

Analysis Procedures. Samples were removed from the fermentor daily and prepared for later analysis. Total dry weights (mycelium and cellulose) were determined by filtering 10 mL samples, washing with an equal volume of water, and drying at 55°C for 24 hr. For estimation of mycelium dry weight, 1 mL samples were spun at 13,600g for 5 minutes, washed with an equal volume of water, and stored at -4°C. Cellular protein was measured by a modified Lowry method (Mohagheghi, 1993) with bovine serum albumin used as a standard. A scale factor of 0.301 (g protein per g dry cell mass) was determined from a xylose fermentation and used to calculate mycelium dry weight. Cellulose concentration was obtained by subtraction of calculated mycelium dry weight from measured total dry weight. Cellulase activity was measured as international filter paper units (IFPU) per mL using the method recommended by the International Union of Pure and Applied Chemistry (Ghose, 1987). Reducing sugar levels were estimated by the dinitrosalicylic acid (DNS) method (Ghose, 1987). Oxygen partial pressure in the fermentor exit gas was determined with a paramagnetic oxygen analyzer (Model E2, Beckman Instruments, Fullerton, CA) capable of detecting 0.05% changes in the range 0–25% oxygen.

Determination of Geometric Constants for Testing with Vane Geometry. The geometric calibration constants for our vane-and-cup geometry were determined using two fluids (one Newtonian and one non-Newtonian) of known rheological character. The details of the calibration process (Bongenaar et al., 1973; Metz et al., 1979) are summarized here.

The correlation between the power number and the Reynolds number for a mixed system in the laminar flow regime is

$$N_P = \frac{c}{N_{Re}} \tag{4}$$

where N_P is the power number, N_{Re} is the Reynolds number, and c is a dimensionless geometric constant. The power number is defined as

$$N_P \equiv \frac{P}{\rho_l N^3 D_i^5} \tag{5}$$

where P is the power input (dyn·cm/s), ρ_l is the density of the liquid under consideration (g/cm^3), N is the rotational speed of the impeller (1/s), and D_i is the diameter of the impeller (cm). The Reynolds number is defined as

$$N_{Re} \equiv \frac{\rho_l N D_i^2}{\eta} \tag{6}$$

where η is the apparent viscosity of the fluid under consideration (p). The power input is related to the torque on the impeller, M (dyn·cm), and the rotational speed, N, by

$$P = 2\pi N M \tag{7}$$

Combining equations 4 through 7 we arrive at

$$\eta = \frac{2\pi M}{cND_i^3} \tag{8}$$

By definition, viscosity is the ratio of shear stress to shear rate. In terms of average values, we have

$$\eta \equiv \frac{\tau_{avg}}{\dot{\gamma}_{avg}} \tag{9}$$

According to Metzner and Otto (Metzner and Otto, 1957), the average shear rate in the vicinity of an impeller can be written as

$$\dot{\gamma}_{avg} = kN \tag{10}$$

where k is a dimensionless constant which depends only on the geometry of the system. Combining equations 8 through 10 we arrive at

$$\tau_{avg} = \left(\frac{2\pi k}{cD_i^3}\right) M \tag{11}$$

Equations 10 and 11 define the average shear rate and average shear stress respectively, in terms of the easily measured physical variables of impeller rotational speed and torque. Thus, given the geometric constants c and k, we can measure N and M for an unknown fluid, and determine its rheological behavior.

To determine the value of c for a vane or impeller, data for torque versus speed must be obtained for a Newtonian fluid (the viscosity of a Newtonian fluid is independent of shear rate, and thus independent of rotational speed) of known viscosity and density. Equation 4 indicates that a plot of log N_P verses log N_{Re} has slope –1.0 and intercept log(c).

Determination of the second geometric constant, k, requires use of a non-Newtonian power law fluid of known rheological character. Choosing the power law of Ostwald–de-Waele given in equation 1, we substitute equation 11 for τ and equation 10 for $\dot{\gamma}$, to yield

$$M = AN^n \tag{12}$$

where the constant A is defined as

$$A \equiv \frac{cKD_i^3 k^{n-1}}{2\pi} \tag{13}$$

Thus, a plot of log M verses log N will have an intercept of log A and a slope of n. The constant k can then be calculated from the value of A since all other variables in equation 13 are known

Dynamic Shear Experiments and Viscoelasticity. Analysis of dynamic oscillatory shear measurements have been given in the literature (Ferry, 1980; Bird et al., 1987)

and are briefly summarized here. In these tests, a sinusoidal deformation, $\gamma = \gamma_o sin(\omega t)$, is imposed on the sample at either a fixed frequency (ω) or strain amplitude (γ_o). The resulting oscillatory stress, τ_{yx}, has components given by (Bird et al., 1987)

$$\tau_{yx} = G'\gamma_o sin(\omega t) + G''\gamma_o cos(\omega t) \tag{14}$$

The stress component in phase with the deformation defines the storage or elastic modulus, G', indicative of the material elasticity. The stress component out-of-phase with the strain defines the loss or viscous modulus, G". The ratio and magnitude of these moduli are sensitive to the microstructure of the system (Bird et al., 1987; Aranguren et al., 1992; Chan, 1985; Khan and Zoeller, 1993).

Rheological Apparatus and Procedure. In all our experiments, we used a Rheometrics Mechanical Spectrometer (RMS-800) capable of both steady and dynamic shear testing. Existing rheometer mountings are used to hold a specially designed vane-and-cup geometry. The vane consists of four blades mounted at right angles to each other; each blade is 40 mm high and 17.9 mm wide. The cup has an inside diameter of 47.6 mm and a working volume of approximately 90 mL.

For rheological analysis, 100 mL of cell suspension were placed in a wide mouth bottle, inverted several times (to remove gas bubbles from the sample), and immediately loaded in the cup. The vane was inserted into the sample so that the top of the vane matched the top of the liquid level and four preprogrammed tests were run: (1) frequency sweep (strain held constant at 1%), (2) strain sweep (frequency held constant at 4 rad/sec), (3) steady shear test (shear rate stepped down from 10 s^{-1} to 0.1 s^{-1}) and (4) a second steady shear test (shear rate stepped up from 0.1 s^{-1} to 10 s^{-1}). In this shear rate range, visual inspection during testing showed no appreciable deformation of the sample surface. All tests were performed at 25°C.

2.5 Results and Discussion

2.5.1 Calibration of Our Vane and Cup Geometry.

We calibrated our vane-and-cup geometry using the procedure described in the Materials and Methods section. In the first step of the calibration process we chose silicone oil (200 Fluid, Dow Corning, Midland MI) as a model Newtonian fluid. All calibration tests were run at 23°C, where the oil's respective density and viscosity were 0.862 g/cm^3 and 1.724 poise (as measured with cone-and-plate geometry). A plot of power number versus Reynolds number for silicone oil in our vane-and-cup system is shown in Figure 1. The low Reynolds numbers and linearity indicate laminar flow, and the data are well represented by the equation

$$N_p = 212 {N_{Re}}^{-1} \tag{15}$$

Thus, from equation 4, $c = 212$. In the second calibration step, we used a cone-and-plate geometry to determine the power law consistency, K, and the power law index, n, of an aqueous solution of 0.4(w/v)% xanthan gum to be 16.24 and 0.240, respectively. The same solution was loaded in our vane-and-cup, and a plot of torque versus rotational speed is shown in Figure 2. In this figure, the relationship $M = 3733N^{0.279}$ best fits the data, and thus from equation 12, $A = 3733$. Using equation 13, and the values determined for c, K, n, and A, we calculated the second geometric constant for our vane-and-cup, $k = 12.48$.

To check our calibration, a portion of the above xanthan solution was diluted with water to a new, unknown concentration. A concentric cylinder geometry was used to determine the power law parameters K and n for the new solution to be 14.41 and 0.32, respectively. A fresh portion of this new solution was tested in the vane-and-cup, and found to have power law parameters K and n of 14.11 and 0.30 respectively. Thus, the power law consistency and index showed differences of only 2% and 5% respectively, between determinations in a conventional geometry and our vane-and-cup. The vane system was used to obtain all rheological results reported in this paper.

2.5.2 Steady Shear Rheological Testing of Fermentation Samples.

The apparent viscosity versus shear rate behavior of a typical fungal-cell/cellulose suspension is shown in Figure 3a. The test sample was taken from a fermentation with 5.0% initial cellulose, 1.3 days after inoculation. The strong shear thinning nature of these suspensions is evident: the apparent viscosity falls by a factor of approximately 40 as the average shear rate increases 100 fold. To illustrate the implications for mixing, we make use of the fact that for most fermentors the geometric constant k (equation 10) falls in the range 10 to 13 (Stanbury and Whitaker, 1984). Thus, at an operational speed of 250 rpm, The average shear rate in the fermentor is approximately 50 s^{-1}. At increasing radial distances from the impeller tips the shear rate falls considerably below the average, and thus the apparent viscosity increases substantially. Regions behind baffles and piping will have even lower shear rates and thus higher apparent viscosities; the possibility for substantial mixing non-uniformity is evident.

All fungal suspensions exhibited similar non-Newtonian, shear thinning behavior to that shown in Figure 3a. A plot of the same data on different axes (Figure 3b) shows that shear stress (τ) increases non-linearly with shear rate ($\dot{\gamma}$); a yield stress is also strongly suggested. To determine whether the power law, Casson, or Herschel-Bulkley model best represented this steady shear data, the experimental results were fitted by each of these models. The Casson and Herschel-Bulkley models in Figure 3b strongly overlap, and both models represent the data much better than the power law. We chose to use the Casson model to represent all additional data because of its prevalence in the fungal fermentation literature.

In all fermentations, both increasing and decreasing steady shear rate tests were performed on each of our suspension samples. Casson model parameters fitted from these individual sweeps typically show less than 5% deviation from each other, and the model–fit error for all fermentation samples is similar to that shown by the error bar in Figure 4b. In addition, when Leong-Poi and Allen (Leong-Poi and Allen, 1992) used a vane-and-cup system similar to ours to measure the yield stress of a different filamentous fungal suspension (*Aspergillus niger*), they obtained values similar to those found here.

When *T. reesei* was grown on particulate cellulose, the fermentation broth passed through three distinct stages. In the first day, just after inoculation, the broth was white and non-viscous. If left unmixed, the solids settled quickly. Then, as cell mass increased, small (< 0.5 mm), very diffuse flocs appeared, the broth began to change to a yellow color, and viscosity increased significantly. After the first day no settling of cell/cellulose suspension was apparent. Flocs remained until substrate was consumed, at which time the suspension became more homogeneous, appreciably less viscous, and grey in color.

2.5.3 Fermentation on Soluble Substrate.

It was desirable for reference purposes to conduct a preliminary *T. reesei* fermentation on a soluble substrate. A fermentation with 4% initial xylose as the sole carbon source (i.e. no particulate solids) was performed, and the evolution of dry cell mass, cellulase activity, and reducing sugar concentration is shown in Figure 4a. Cell mass rose to a single maximum and xylose was completely consumed after a period of 3 – 3.5 days, after which biomass concentration showed a slight decline for the remainder of the fermentation. Cellulase enzyme activity rose linearly, but only after xylose exhaustion. The steady–shear Casson yield stress and viscosity for samples from this fermentation are presented in Figure 4b. Both parameters increased as biomass grew. The broad maxima in yield stress and biomass coincided, approximately 3 days after inoculation, while the Casson viscosity showed a slightly earlier maximum. Then, as biomass concentration declined somewhat in the latter half of the fermentation, the yield stress and the Casson viscosity declined more strongly and the correlation between cell mass and Casson parameters disappeared. Microscopy revealed (data not shown) that cellular morphology had changed significantly at the end of the fermentation (Velkovska, 1995): cells were heavily sporulated and significant lysis of the hypha had taken place, resulting in microstructural breakdown and thus substantial decreases in yield stress and Casson viscosity.

2.5.4 Oxygen Limited Fermentation

In all fermentations using cellulose carbon source, the initial concentration was 50 g/L. This concentration has been reported (Mohagheghi et al., 1988; Hendy et al., 1982) to

produce maximum cellulase activity in *T. reesei* batch fermentations.

Anticipating that cellulase–activity production in *T reesei* fermentations might be sensitive to impeller shear (Mohagheghi, 1993), we first used impeller tip speeds below 100 cm/sec (approx 250 rpm). To determine if fermentations at this relatively slow impeller speed lead to oxygen mass–transfer limitations, and potentially detrimental effects on cell growth and cellulase production, we conducted a fermentation using air only as the fermentation inlet gas. Data for dry cell mass, substrate cellulose, and product cellulase–activity are shown in Figure 5a. From this plot it appears that fungal cell growth proceeded in two stages: During the first day, dry cell mass showed a rapid rise from an initial value of approximately 3 g/L to approx 8 g/L. This rise was then followed by slower growth, with cell mass reaching approximately 14 g/L after 7 days. This maximum corresponded with cellulose exhaustion and the onset of heavy sporulation, as identified by microscopy. Product cellulase activity rose to only 1.4 IFPU/mL by the end of the fermentation.

Casson model parameters for this experiment (Figure 5b) show similar behavior to those from the fermentation on soluble substrate (Figure 4b). Both yield stress and Casson viscosity increased over the course of the experiment, showing maxima nearly corresponding with the maximum in dry cell mass. Yield stress peaked at about 20 dyn/cm^2, almost double that for the xylose fermentation, while Casson viscosity rose to 12 p$^{1/2}$, a value similar to that for xylose. The cellulose suspensions themselves are reported as having low viscosity with nearly Newtonian behavior. Ang (Ang, 1991) found that powdered cellulose, with the same fiber length as used in this study, did not appear to have any thickening properties when suspended in water at concentrations of 3.0%. With our vane-and-cup system, a 5% cellulose suspension had an apparent viscosity below the measuring range of our rheometer. Thus, results shown in Figure 5b can clearly be attributed to the fungal suspension.

During the the early stages of this air–only experiment, while the DO level was high (Figure 6a), we halted air sparging for a short time and maintained fermentor headspace pressure constant (2 psig). A critical dissolved oxygen concentration (C_{crit}) of 15% (0.073 mmol O_2/L) was determined from the declining DO versus time trace (point where trace deviated from linearity (Stanbury and Whitaker, 1984), data not shown) and is in agreement with that found by others (Rakshit and Sahai, 1991). This technique was repeated in several subsequent fermentations and consistent results were obtained. Figure 6a shows that the DO concentration fell below C_{crit} during the second day of the fermentation, implying achievement of oxygen–limited cell growth.

The volumetric oxygen transfer rate (N_A) was determined by an oxygen balance technique (Wang et al., 1979), for this and subsequent experiments, and the mass transfer conductance ($k_l a$) was determined from equation 16:

$$k_l a = \frac{N_A}{C^* - C_l} \tag{16}$$

where $k_l a$ is in hr^{-1}, N_A is in mmol O_2/L·hr, C^* is the broth dissolved oxygen concentration

in equilibrium with the exit gas, and C_l is the concentration of dissolved oxygen in the fermentation broth. Figure 6b shows that the fall in k_La, from its high initial value to approx 300 hr^{-1}, coincided with the decrease in DO concentration, 1.5 days after inoculation.

2.5.5 Oxygen Supplemented Fermentations

In subsequent fermentations, oxygen mass–transfer limitations were avoided by supplementing inlet air with pure oxygen. We performed four *T. reesei* experiments with this air/oxygen feed configuration at a fermentor impeller speed of 250 rpm. In all experiments, curves for cell mass, cellulose substrate, and cellulase activity show almost identical behavior. In addition, cell growth in all four experiments proceeded in two stages: rapid initial growth during the first day, followed by slower growth and achievement of a maximum biomass level when cellulose was consumed. Results from two of these experiments (Figures 7a and 8a) show that dry cell mass rose from 3 g/L to approximately 13 g/L during the first two days of growth, then increased more slowly until a maximum of approximately 22 g/L was reached after 6 days. This maximum is almost triple that achieved in the oxygen limited fermentation (Figure 5a). Cellulase activity rose slowly at first then increased to approx 3.5 IFPU/mL, almost triple the level in the oxygen limited experiment. The low value of the final two cellulase–activity data in Figure 7a result from dilution caused by excess liquid addition (acid/base) for pH control.

A possible explanation for the bi-phasic cell growth shown in these cellulose fermentations is that the amorphous cellulose portion of Solka Floc in the growth medium was easily hydrolyzed, and thus consumed first. This rapid growth phase was then followed by hydrolysis of the more recalcitrant micro-crystalline cellulose portion of the Solka Floc and slower growth. To test this hypothesis, we performed a fermentation with pure micro-crystalline cellulose (Sigmacell, Sigma Chemical) as sole carbon substrate (Figure 9). While the final cell–mass maximum was lower than in Solka Floc fermentations, the fast and slow growth stages remain. A second and more likely explanation for bi-phasic growth, is that the 10 g/L initial yeast extract in the growth medium was quickly converted to cell mass, and accounted for the 10 g/L increase during the first two days of growth. The second, slower growth phase was then dominated by the hydrolysis and consumption of cellulose.

Casson model parameters from all four oxygen-supplemented fermentations showed dual maxima in both yield stress and Casson viscosity. Results from two of these experiments are shown in Figures 7b and 8b, where the first maximum for both parameters appears just as biomass completes its rapid initial increase (1.5 days), and the second occurs just before the maximum biomass concentration (5 days). The occurance of the maxima, and the strong correlation between yield stress and Casson viscosity, were very reproducible, but the maximum levels achieved varied somewhat. The dual maxima suggest that even though biomass concentration may be the dominant factor governing variation in Casson model parameters, cell morphology also plays a significant role, as found with other fungal systems

(Tucker et al., 1993; Olsvik et al., 1993).

To maintain DO concentration above C_{crit} and below what might have been inhibitory values (> 100% air saturation), we used a galvanic DO probe connected to a gaseous oxygen controller (Model 508, LH Fermentations). The controller opened a solenoid valve, adding pure oxygen to the air feed stream, whenever the broth DO fell below 20%. Three flowmeters were used to control the relative amounts of air, oxygen, and inlet–gas so that the fermentor sparge rate was held constant whether the solenoid was open or closed. Figure 10a shows that the broth DO level during the Figure 7 experiment remained above C_{crit} for the entire fermentation. Because the solenoid was opening and closing frequently in this experiment, the inlet oxygen concentration was constantly changing, and it was not possible to determine N_A via the oxygen balance technique. Hence it was not possible to calculate $k_l a$. Instead, the solenoid was connected to a chart recorder, and the total oxygen (air + pure O_2) added to the fermentor was recorded. Since the solenoid opened in response to the oxygen demand of the cells, the total oxygen feed rate (OFR) reflects the cellular oxygen demand. The OFR and Casson viscosity for one of the four fermentations at 250 rpm (Figure 10b) show corresponding dual maxima, indicating that the increased Casson viscosity caused a decrease of $k_l a$, and thus cells required an increased OFR.

2.5.6 Fermentations at Elevated Impeller Speeds

To explore for possible shear sensitivity of this *T. reesei* strain, we performed experiments at impeller speeds of 400 (Figures 11 and 12) and 550 rpm (Figures 13 and 14). Similar to the 250 rpm experiments, the cell mass curves in both cases (Figures 11a and 13a) showed two phase behavior. A rapid initial rise of approx 10 g/L was followed by somewhat slower growth and a maximum achieved at 22 g/L, coinciding with cellulose exhaustion. In contrast to the 250 rpm experiments, this maximum was reached after only 4 days in the 400 rpm experiment and after only 3 days in the 550 rpm fermentation. The final cellulase activity in the 550 rpm experiment reached a level of 5.5 IFPU/mL, 60% greater than that typically achieved in the 250 rpm runs.

In the 400 rpm fermentation, both yield stress and Casson viscosity versus time showed behavior approaching a single maximum (Figure 11a), while at 550 rpm both parameters clearly showed only a single maximum (Figure 13a). In addition, both parameters reached higher values at these elevated impeller speeds than at 250 rpm. Casson viscosity reached a maximum of approx 1.2 at both 400 and 550 rpm, compared to only 0.8–0.9 at 250 rpm. Yield stress maximums not only increased, but occurred earlier with increasing impeller speed. Figure 15 shows yield stress versus time data for 250, 400 and 550 rpm reached maxima of 15, 33 and 52 dyn/cm^2, respectively. Microscopy showed somewhat shorter mycelia at 400 and 550 rpm than at 250 rpm, but the difference was not pronounced. It is unclear how the shorter mycelium observed at the higher impeller speed led to greater values of yield stress and Casson viscosity. We offer two possible explanations. The higher impeller speeds

may have caused more cells to lyse, thus releasing cytoplasmic components that allowed ionic interaction with remaining cells to stabilize the broth microstructure. Alternatively, the higher shear environment may have led to more rigid hypha that interacted with each other to stabilize microstructure which led to higher yield stress values.

The well mixed region surrounding the impeller in a yield stress fluid was first described as a "cavern" by Wichterle and Wein (Wichterle and Wein, 1979), who proposed an expression for cavern diameter as function of the fluid yield stress. Solomon (Solomon et al., 1981) observed caverns visually and with hot wire anemometry, and presented a spherical cavern model centered around the impeller. This model was modified by Elson et al. (Elson, 1988; Elson, 1990) who proposed existence of a right circular–cylinder shaped cavern, which maintained approximately constant shape and aspect ratio. For a six bladed disc turbine (similar to that used here) in the laminar flow regime, the cavern size is approximately equal to the volume swept out by the impeller. In the transition and turbulent flow regimes, the cavern size increases with rotational speed according to:

$$\left(\frac{D_c}{D}\right)^3 = \frac{N_{Pot} N_{Re_y}}{\left(H_c/D_c + \frac{1}{3}\right)\pi^2} \tag{17}$$

where D_c is the cavern diameter, D is the impeller diameter, N_{Pot} is the turbulent power number, N_{Re_y} is the yield stress Reynolds number ($\rho N^2 D^2/\tau_y$), and H_c/D_c is the ratio of cavern height to diameter. Disc turbines were found to have cavern aspect ratios (H_c/D_c) of 0.4 for $D_c < T$ (tank diameter) (Elson, 1988). Equation 17 has been shown to apply to gassed as well as un-gassed systems as long as the appropriate value of N_{Pot} is used (Nienow and Elson, 1988; Galindo et al., 1988). If equation 17 is rearranged, and tank diameter T is substituted for D_c, we arrive at the equation for N_w, the impeller speed at which the cavern reaches the vessel wall:

$$N_w = \frac{\pi}{D}\left[\frac{\left(H_c/D_c + \frac{1}{3}\right)\left(\frac{T}{D}\right)^3 \tau_y}{\rho N_{Pot}}\right]^{1/2} \tag{18}$$

Equation 17 holds true until the cavern reaches the vessel wall, after which point the cavern height increases with impeller speed according to (Elson, 1988):

$$H_c \propto N^{0.87} \tag{19}$$

We assume that H_c/D_c for our system was 0.4, and separated the three impellers in our fermentor such that the caverns for each impeller just overlapped for $N = N_w$, implying that for $N \geq N_w$ the caverns completely filled the fermentor vessel. Figure 16 shows the calculated N_w as a function of fermentation age for experiments at 250, 400 and 500 rpm. In each of these experiments N_w was almost always significantly below the actual operating speed, and thus none of our fermentations contained stagnant, or completely unmixed regions.

Cells grown at all speeds appeared in what we have termed either primary or secondary forms (Velkovska et al., 1995). Primary cells, as identified by microscopy, were relatively long,

unbranched, and unsporulated, while Secondary cells, which appeared after the second day of growth, were somewhat shorter, more highly branched, and contained chlamydospores. We postulate that primary cells grew initially when yeast extract was available in the growth medium. Then, as this nutrient disappeared, cells began to grow slowly on cellulose in their secondary form. These two cell morphologies may explain the dual maxima found in Casson parameters for cells grown at 250 and 400 rpm.

Figures 12a and 14a show that DO levels in the 400 and 550 rpm fermentations respectively, were maintained above C_{crit}, and thus cells were not oxygen limited. Figures 12b and 14b show that at both speeds, k_La fell from a high initial value as the yield stress increased, then rose as yield stress decreased in the latter half of the experiment. Antifoam addition in the 400 rpm experiment caused substantial decreases in k_La (Figure 12). To avoid this problem in the 550 rpm fermentation, antifoam was only added immediately after inoculation.

2.5.7 Oscillatory Shear Rheological Testing of Fermentation Samples.

To ascertain microstructural changes in broth suspensions over the course of fermentations, we used dynamic rheological measurements. Two tests were run on each sample. The first was a frequency sweep, with oscillation amplitude held constant at 1% and oscillation frequency increased from 0.1 to 10 rad/s. A plot of the elastic (G') and viscous (G") moduli as a function of frequency is shown in Figure 17. The sample used for this test was removed from a 5% initial cellulose fermentation, 1.3 days after inoculation. We find both moduli to be relatively "flat," and G' to be larger than G", indicating that the cell suspension behaved as a gel (Aranguren et al., 1992; Khan and Zoeller, 1993; Khan et al., 1994). The shape of these curves are representative of frequency sweeps of all samples in all fermentations performed.

The second oscillatory shear experiment on each sample was a strain sweep, where the frequency was held constant at 4 rad/s and the oscillatory strain amplitude was increased from 0.3% to 80%. The results of a typical strain sweep are shown in Figure 18 (same sample used for the frequency sweep of Figure 17). Both G' and G" show "plateau" behavior at strain (γ) values below approx 1%, thereby identifying the linear viscoelastic region. In this regime G' > G", indicating the presence of a network structure, thus corroborating the results from the low strain–amplitude frequency sweep. With increasing strain, G' decreases and eventually equals G", indicative of microstructural breakdown. This behavior has been observed in various systems with internal structure (Aranguren et al., 1992; Khan and Zoeller, 1993)

Figure 19 shows the evolution of G' and G" strain sweep plateau values as a function of fermentation age for three *T. reesei* fermentations with impeller speeds of 250, 400, and 550 rpm. For all fermentations the moduli histories exhibit almost identical shape, with G'

greater than G". The dynamic moduli at all three speeds behave similarly to the Casson parameters from corresponding experiments (Figures 8a, 11a, and 13a), thus showing the relationship of broth microstructure to mycelial cell mass and the simple constitutive equation. To illustrate the strong correlation between the steady and dynamic shear variables more clearly, yield stress values from nine different fermentations are plotted as function of G' in Figure 20. This curve shows excellent linear correlation between yield stress and G'.

The loss tangent, defined as the ratio of the viscous to elastic modulus (tan $\delta \equiv$ G"/G'), is a measure of material microstructure. For all fermentation samples, the loss tangent is less than one for all fermentation ages. Thus, our fungal suspensions preserve their "gel-like" nature (tan $\delta < 1$) throughout the fermentation. Although tan δ remains approximately constant over the course of each fermentation, the magnitude of the individual dynamic moduli undergo significant changes with time.

2.6 Conclusions

Geometric constants determined for the vane-and-cup rheometer geometry used in this study compare well with those for similar systems described in the literature (Metz et al., 1979; Kemblowski and Kristiansen, 1986; Allen and Robinson, 1990). In addition, power law parameters generated for a xanthan gum solution with our vane-and-cup showed close agreement with power law parameters determined with a conventional, concentric cylinder geometry, validating use of our vane system for measuring rheological behavior of fungal cell and cellulose mixed suspensions. The Casson model and the Herschel-Bulkley model represented *Trichoderma reesei* broth steady shear behavior better than the power law, despite suggestion (Reuss et al., 1982) that the latter is equally suitable for correlation of fungal rheology.

Biomass concentration is known to be the dominant factor governing the rheological behavior of other fungal species (Tucker et al., 1993; Olsvik et al., 1993). In the present study, biomass concentration profiles exhibited either unimodal or bimodal behavior versus time depending on the substrate (soluble xylose or particulate solid cellulose). When *Trichoderma reesei* are grown on cellulose (Solka Floc), a rapid initial biomass growth occurs, apparently due to availability of yeast extract in the growth medium. Later, when sufficient cellulase is present, the cellulose hydrolysis rate rises substantially to support a second growth phase on the more recalcitrant cellulose fraction. The second growth phase halts when cellulose is consumed.

Cells grown at 250 rpm, and sparged with air only were oxygen limited and showed low biomass concentration and final cellulase activity when compared with cells grown in oxygen supplemented air. The critical dissolved oxygen (DO) concentration, C_{crit}, was determined to be 0.073 mmol O_2/L. The broth DO was maintained above this level to prevent oxygen limitations.

In all fermentations, Casson model parameters strongly reflected biomass variation, showing a single broad maximum when cells were grown on xylose, dual maxima when cells were grown on cellulose at low speed, and a single maximum at higher fermentor impeller speeds. Increased fermentor impeller speed led to higher maximum yield stress at earlier fermentation times.

Dynamic, oscillatory shear measurements showed consistent, low-strain (< 1%) "gel-like" behavior and high-strain (> 10%) liquid like behavior for all suspensions, independent of concentration and time. This implies there could be substantial mixing non-uniformity in large scale *T. reesei* fermentations. The low strain, time-dependent variation with fermentation time of both the elastic (G') and viscous (G") moduli were similar to the bimodal trend found for biomass, corroborating the steady shear data.

3 Kinetic Model for Batch Cellulase Production by *Trichoderma reesei* RUT-C30 (A paper submitted to *Journal of Biotechnology*)

3.1 Abstract

A kinetic model for batch cellulase enzyme production by *T. reesei* from cellulose substrate is constructed from literature concepts and laboratory data. The key concepts included were four:

1. existence of primary and secondary mycelia
2. cellulase production by secondary mycelia only
3. the adsorption of cellulase (catalyst) on the particulate cellulose (substrate), and
4. the decline of cellulose reactivity with extent of conversion

The laboratory batch data were biomass (particulate), substrate (particulate cellulose), and product (cellulase enzyme and reducing sugar) concentration vs. time. The kinetic parameters were evaluated simultaneously through a nonlinear fitting routine, and the resultant model is shown to fit the data well. The model's success validates the presumed need to include all four concepts in reactor analysis for cellulase production.

3.2 Symbols Used in Chapter 3

A	activity of adsorbed enzyme, IFPU g cellulose^{-1}
A_{max}	maximum activity of adsorbed enzyme, IFPU g cellulose^{-1}
E	enzyme activity in the fermentation broth, IFPU ml^{-1}
E_{ad}	activity of the adsorbed cellulase enzyme, IFPU ml^{-1}
E_f	free cellulase enzyme activity in the system, IFPU ml^{-1}
ES	concentration of cellulose-cellulase complex, IFPU ml^{-1}
E_t	total cellulase enzyme activity in the fermentation system, IFPU ml^{-1}
K_{ad}	adsorption equilibrium constant, ml IFPU^{-1}
k_d	combined death and endogenous maintenance specific rate constant, d^{-1}
K_s	saturation constant of the primary mycelium, g l^{-1}
$K_{s,s}$	saturation constant of the secondary mycelium, g l^{-1}
k_1	specific rate constant for transformation of primary into secondary mycelium, d^{-1}
k_2	enzyme synthesis rate constant, IFPU g cell^{-1} d^{-1}
k_3	enzyme decay rate constant, d^{-1}
k_4	hydrolysis rate constant, d^{-1}
k_5	exponent of the declining substrate reactivity, dimensionless
k_6	conversion -independent component in rate function, d^{-1}
μ_m	specific growth rate of the primary mycelum, d^{-1}
$\mu_{m,s}$	specific growth rate of the secondary mycelium, d $^{-1}$
r	hydrolysis rate, g l^{-1} d^{-1}
S	substrate concentration, g l^{-1}
S_o	initial cellulose concentration in the fermentation broth, g l^{-1}
t	time, day
x	cellulose conversion, dimensionless
X_p	primary mycelium concentration, g l^{-1}
X_s	secondary mycelium concentration, g l^{-1}

3.3 Introduction

Cellulase production provides catalyst for cellulose hydrolysis to glucose, to be used for eventual production of ethanol. The production of cellulase enzymes with a batch fermentation of the fungus *Trichoderma reesei* is dependent on many factors, as the *Trichoderma* cellulase system is of a complex nature. Complete quantitative description of its kinetic behavior requires not only mathematical expressions describing the time course of each important variable (substrate, biomass and enzyme concentration), but also inclusion of known, important aspects of fungal cell physiology, enzyme adsorption, and substrate reactivity.

In prior kinetic models for cellulase production several factors have been considered: pH of the medium (Brown and Halsted, 1975; Rakshit and Sahai, 1991; Chanal et al., 1992), oxygen supply (Brown and Zainudeen, 1977), type of substrate and its concentration (Sternberg and Dorval, 1979; Mohagheghi et al., 1988; Mohagheghi et al., 1990; Schafner and Toledo, 1992; Chanal et al., 1992), and type of operation (Mitra and Wilke, 1975; Ghose and Sahai, 1979; Hendy et al., 1982), etc. Most of these studies examined the kinetics of enzyme production from soluble substrates, only a few (Ghose and Sahai, 1979; Rakshit and Sahai, 1991; Bader et al., 1993) used an insoluble substrate (cellulose). Important factors not all included in prior models, and which may influence the kinetics, are (i) existence of different cell forms and their influence on growth rate and product formation, (ii) product (cellulase) adsorption on insoluble substrates (such as cellulose), and (iii) cellulose reactivity which varies with extent of conversion.

During the growth and development of *Trichoderma reesei* cells, several morphological and physiological changes take place. These changes (long hyphae appearance, sporulation, etc.) influence cellulase production and need to be taken into consideration in a batch model. Little information is available concerning specific biochemical factors which determine the existence of and transitions between the cell growth phases and their respective connections with the production kinetics. This paper therefore develops a model which is structured in biomass and substrate reactivity variables, but unstructured as regards intracellular mechanisms and molecular species.

Cellulase enzymes adsorb on the substrate cellulose, and many studies show that a significant fraction of cellulase is adsorbed during hydrolysis (Oosima et al., 1990; Kim et al., 1992; Obraztsova et al., 1993). We investigated the adsorption behavior of *T. reesei* cellulase enzymes, and show that the Langmuir adsorption isotherm adequately represents this phenomenon.

Previous literature models for cellulase production do not give a complete picture of the system. The model of Rakshit and Sahai (1991) defines cell growth and cellulase formation, but does not include substrate consumption. For cell growth these authors used the generalized logistic model, which serves conveniently for mathematical fitting, but not for a physical, substrate-dependent definition of cell growth.

Ghose and Sahai (1979) proposed a very simple model for biomass, substrate and product changes in fed-batch and continuous systems, without taking into account the either enzyme adsorption or the two distinct forms of biomass cited above. Their model was not compared to experimental data.

Other studies give a complete picture of cellulase production with *Trichoderma reesei*, when the soluble substrates glucose or xylose were used (Brown and Halsted, 1975; Mitra and Wilke, 1975; Brown and Zainudeen, 1977; Schafner and Toledo, 1992).

The most complete cellulose substrate model to date is that of Bader et al. (1993). These authors modeled enzymatic hydrolysis data of Klingspohn et al. (1993) for *T. reesei* RUT C30 grown on depectinized potato pulp (cellulose/hemicellulose), pulp residue (depectinized pulp followed by enzymatic pretreatment), and cellulose. A detailed kinetic network was described including production of the individual enzymes exoglucanase, endoglucanase, and xylanase, as well as "new" and "old" cells. Only new cells were assumed to be productive of enzymes (synthesis rate thus proportional to total biomass), and they were capable of substrate uptake, as indicated below:

$$\begin{array}{ccccc} & & enzymes & & \\ & & \uparrow & & \\ S & \rightarrow & X_{new} & \rightarrow X_{old} \rightarrow & inactive \end{array}$$

Simulations were compared with data, for individual enzymes and for total dry weight (cells plus particulate substrate(s)); individual biomass and cellulose data were not available.

For batch cultivation of *T. reesei* RUT C30 on particulate cellulose, the present paper presents a complete model which is simpler than that of Bader et al. (1993) with respect to enzyme product but which includes for the first time direct comparison with our own data for substrate (cellulose), catalyst (biomass), and product (cellulase). Key differences between the recent Bader et al. model and ours are as follow:

1. only the secondary (new) cells are assumed to produce hydrolytic enzymes.
2. Bader et al's model (1993) found satisfactory fit to enzyme data when the relative enzyme synthesis rates for exoglucanase, endoglucanase, and xylanase remained constant. We therefore model only total enzyme, since the "composition" of the hydrolytic enzyme mixture actually synthesized is assumed to remain constant.
3. To include variable substrate reactivity with conversion (including changing ratios of amorphous to crystalline cellulose, variable deactivation rates among different enzymes, etc.), we include a variable substrate reactivity model of South et al. (1994).

Rakshit and Sahai (1991) have reported an absence of oxygen mass transfer influence during the cellulose fermentation if the dissolved oxygen (DO) level is maintained above 15%

of air saturation. We examined mass transfer limitations for better process characterization, but all experiments for modeling in the present paper were run at DO levels above 20% of air saturation. Hence DO is not a model variable. Results from oxygen mass transfer and rheological studies of *T. reesei* culture broths are presented elsewere (Marten et al., 1995).

In the following sections we describe our experiments and the development of a mathematical model which includes cell growth, substrate utilization and cellulase production kinetics.

3.4 Materials and Methods

Microorganism. *Trichoderma reesei* RUT-C30 was used in this investigation, and was maintained on potato-dextrose agar.

Culture Medium and Cultivation. Growth and production conditions were described earlier (Mohagheghi et al., 1988; Mohagheghi et al., 1990) with slight modifications (Mohagheghi, 1993). Successive 50 ml, then 1000 ml inocula were grown on 10 g/L glucose and 10 g/L insoluble Solka Floc 200 FCC cellulose (35 μm fiber length, Fiber Sales and Development Corp., Urbana, OH) respectively, at 28°C on an oscillating shaker (225 rpm). The fermentations were carried out in the 16 liter steam sterilizable fermentor (Microgen SF116, New Brunswick Scientific), at 28°C, with an impeller speed of 250 rpm and pH=4.8. Air, with oxygen supplement, was sparged at 0.2-1.0 VVM, to provide an average broth dissolved oxygen concentration of 35±15 %, except under extreme growth when DO fell below 20%.

Analytical Methods. Enzyme activity was determined using the filter paper (FPA) assay, while reducing sugars were measured by the dinitrosalicylic acid (DNS) method. Individual sugar concentrations were analyzed by high performance liquid chromatography (Perkin Elmer HPLC, 250x4.1 mm Microsorb MV (Rainin) amino column, at 25°C with RI-detector). The mobile phase was 70% acetonitrile with a flow rate of 1.8 ml/min. Pure glucose, xylose and cellobiose were used as standards.

Total dry weight measurements were performed to determine the amount of cellulose plus dry cells in the system. Mycelium dry weight was estimated by measuring the total protein mass with the modified Lowery method (Mohagheghi, 1993) (Bovine serum albumin as a standard) and multiplying by the ratio of dry cell mass to protein for *T. reesei*. This conversion factor was estimated from data for dry cell and protein concentrations in a xylose fermentation, where cells were the only insoluble component. Cellulose concentration at any time was determined as total dry weight minus estimated dry cell mass.

Determination of Adsorption Isotherm. The adsorption of cellulase was examined by contacting fermentation broth filtrate samples of known enzyme activity with fresh Solka Floc 200 FCC cellulose as adsorbent. Significant amounts of cellulase were found to

adsorb on the cellulose.

The procedure for determination of the adsorption isotherm was a modification of that proposed by Kim et al. (1992). Cellulose samples (50 mg and 150 mg) were suspended in 1.0 ml of 0.1 M sodium acetate buffer (pH=4.8) in test tubes, and preincubated at 28°C for 30 minutes. After preincubation, 4 ml of fermentation broth filtrate, with various enzyme activities (0.065-3.350 IFPU/ml), were added to the treated cellulose samples. The reaction mixture was subjected to reciprocal shaking at 200 rpm for 30 minutes, sufficient time to attain adsorption equilibrium, then centrifuged for 5 minutes at 5000 rpm. The equlibrated supernant enzyme activity was determined with the filter paper assay, and data were fitted to a Langmuir adsorption isotherm.

3.5 Results and discussion

3.5.1 Model Development

Cellulase production can be defined as a Type III fermentation, as defined by Gaden (1955). In the biosynthesis reaction, the main product apparently does not result from energy metabolism, and is elaborated independently by the cells, as shown by our data in Figure 21 and 22.

During this type of fermentation, two phases are noticeable: primary and secondary (Gaden, 1955). In the primary phase, biomass accumulation and normal metabolic activities reach their maximum, then in the secondary, later phase, product accumulation and formation rate reach their maximum values. Specific growth rates were estimated using the data of Figure 21 and fitting to 7th order polynomial curves, accurate enough to reach correlation factor r^2 for all three curves of 0.98. Differentiation provides specific rates for cellulase utilization, cell growth, and product (cellulase) synthesis (Figure 22).

All our cellulose fermentations showed similar kinetic features, and the challenge was to give an explanation and to develop a mathematical model consistent with those findings.

A related fermentation pattern was observed by Doskacil et al. (1958) in the production of oxytetracycline by Streptomyces rimosus in submerged culture. They divided the fermentation into 5 stages. The first stage was lag phase (not observed in our studies of cellulase fermentation, due to our use of substantial inoculate in the exponential phase of growth and addition of yeast hydrolysate with the inoculum). The second stage was characterized with growth of primary mycelium, but no product formation. In the third stage, mycelium growth ceased, and fragmentation of the primary mycelium occurred. The fourth stage was characterized by both rapid product formation and growth of secondary mycelium, whose thin filament morphology differed from that of the primary mycelium. The substrate in this stage was rapidly depleted. In the stationary, fifth stage, growth ceased and product

formation continued, but at a much lower specific rate.

Matsumura et al. (1981) observed a three fold morphological difference between Cephalosporium acremonium cells during cephalosporin C production. The first cell type was a typical hyphal form able to assimilate methionine and glucose. Hyphal branches can swell to become the second type of cell, capable of antibiotic production. The third cell and non-productive type is formed after depletion of glucose in the medium, when the long swollen hyphal fragments shorten and become arthrospores.

The concept of two mycelium forms of *T. reesei* is clearly verified by cell morphology. Microscopic observations were performed to show that our "young" cells of *Trichoderma reesei* in the initial period of fermentation (the first several days) are very long and modestly branched (see Figure 23). Our experimental analysis of the product enzyme titer showed that these filaments are not very active for production of cellulase enzyme. After the fast initial formation of the primary mycelium, microscopic analysis showed that the mycelium structure starts to change after approximately 2-3 days. The changes are characterized by branching of the mycelium and the eventual appearance of chlamydospores. These chlamydospores are actually terminal or intercalary segments of the mycelium, which have developed substantial food reserves and thick walls (Webster, 1980). Chlamydospores form important organs of asexual survival, and usually appear as a result of substrate exhaustion. We assume that our "substrate exhaustion" is due to early disappearance of the easily consumed components introduced with inocula: the reducing sugars and peptones of our yeast hydrolysate, which triggers a physiological transformations (appearance of secondary mycelium) in the cells to survive in medium with cellulose as the only substrate source.

The growth of new, secondary mycelium results in the appearance of an additional peak in the biomass vs. time curve. At the same time, appreciable product formation is detected, similar to the oxytetracycline fermentation. This morphological structure of the secondary mycelium, with little change, remains uniform until the end of the fermentation. The existance of two peaks in the biomass concentration and growth rates was common for all fermentations which we conducted at 250 rpm speed of the impeller. At higher speed the two peaks in the growth curve were less noticeable (400 rpm), and they merged at 500 rpm. However, microscope pictures still showed two kinds of mycelia.

Why do only the secondary mycelium appear to be responsible for the product formation? The fundamental studies of Stavy et al. (1970), found that both in vivo and in vitro , the young growing front of a *Trichoderma reesei* colony is far more active in protein synthesis than is the older core. The microsomes were found to be more concentrated in the young growing front, and these newer microsomes have a higher capacity to carry out protein synthesis than the aged inner core microsomes. As the secondary mycelium is highly branched, with many actively growing hyphal tips, it has much greater capacity for cellulolytic protein synthesis than does the primary cell mass.

3.5.2 Model Features

The *Trichoderma reesei* cellulase-cellulose system is complex. For development of the model equations for cell growth, substrate utilization and product accumulation, the following established features of *Trichoderma reesei* fermentation for cellulase production were taken into account:

- Existence of primary and secondary mycelium;
- Cellulase enzymes are a product from secondary mycelium;
- Product (cellulase) adsorption equilibrium occurs on the particulate substrate (cellulose);
- The cellulose reactivity declines with increased conversion.

Potential enzyme inhibition effects by cellulose degradation products (glucose and cellobiose) are not taken into account, because the measured concentrations of reducing sugars were very low (< 4 g/L) during the entire fermentation. The highest concentration of glucose was observed in the beginning of the fermentation, and this maximum concentration of 1.2 g/L is too low to cause cellulase inhibition (Nutor and Converse, 1991). The maximum concentration of cellobiose was even lower.

3.5.3 Biomass Synthesis Model Equations

For development of the cell growth equation, we consider that two kinds of mycelia are present in the system. The growth of the *T. reesei* fungus is related to the uptake of substrate: directly for the primary and indirectly for the secondary mycelium. In the biomass model equation, only the cellulose is specified as substrate, even though for the brief initial period (first 10-12 hours), major changes in medium protein and reducing sugars concentration were observed due to their consumption.

The reducing sugars dropped from 3.5 to 0.5 g/L within the first 10-12 hours of the fermentation and remained constant at approximately 0.5 g/L thereafter. HPLC Analysis showed glucose to be an average of 30% of the initial reducing sugars. Traces of xylose and cellobiose were also observed, but they were determined only qualitatively because of their very low concentration. The remaining reducing sugars were not identified, either quantitatively or qualitatively. Separate analyses of the inoculum, the pure cellulose and the yeast extract used in the fermentation confirmed the presence of reducing sugars, in a total amount approximately equal to that determined in the earliest stage of the fermentation itself.

Protein concentration also showed a drop for the early stage of cellulase fermentation. Tangnu et al. (1981), explained a similar decline to result from peptone consumption by the cells. We used yeast extract (peptone source) to fulfill the cell requirements for nitrogen.

Both reducing sugars and proteins contribute to the initial fast growth of the biomass. Neither source could be completely defined qualitatively and quantitatively, and for simplification of the model, they were not taken into account. There was no major drop in the cellulose concentration during the initial 10-12 hour period of fermentation, after which the cellulose was consumed. Based on these findings, the usage after several hours of cellulose as the only substrate in the model equation seems reasonable.

For the primary mycelium, we use the following biomass growth and conversion equation:

$$\frac{dX_p}{dt} = X_p \frac{\mu_m S}{K_s + S} - k_1 X_p \tag{20}$$

where μ_m is the specific growth rate, K_s is the saturation constant and k_1 is the specific rate constant for transformation of primary into secondary mycelium. The first Monod term represents the strong dependence of the primary cells growth on cellulose concentration, and the additional term $k_1 X_p$ takes into account the transformation of primary cells into secondary mycelia.

For the secondary mycelia, the following equation is adopted:

$$\frac{dX_s}{dt} = k_1 X_p - k_d X_s \tag{21}$$

where k_d is combined death and endogenous maintenance specific rate constant.

The rate of secondary mycelium accumulation is thus the difference between the rate of secondary cell formation from the primary mycelium, and the combined cell death and endogenous rates, defined with the specific rate constant k_d. In the initial modelling attempt, we included in equation (21) an additional specific growth rate term: a Monod form for substrate utilization by the secondary mycelium: $\mu_{m,s} S X_s/(K_{s,s} + S)$. Non-linear curve fitting of biomass data yielded estimated secondary mycelium specific growth rates ($\mu_{m,s}$) for all fermentations which were 20-100 times smaller then μ_m of the primary mycelium (i.e., $\mu_{m,s} < \mu_m/20$), and the omission of this second Monod term did not influence significantly the model fit. Therefore, we do not include this term in the general model. Matsumura et al. (1981) in their kinetic model for cephalosporin C production also reported much smaller specific growth rate for the secondary vs. primary mycelium, where the second cell form was capable of antibiotic production.

The total biomass concentration X in the fermentation broth is the sum of both mycelia types, and consequently the total rate of biomass formation is sum of the individual

rate equations (20) and (21):

$$\frac{dX}{dt} = X_p \frac{\mu_m S}{K_s + S} - k_d X_s \tag{22}$$

3.5.4 Product Formation

T. reesei synthesizes and excretes diverse enzymes. Cellulase production was previously noted not to result from energy metabolism. The time course of fermentation showed that enzyme formation is correlated to the appearance of secondary mycelia, a fact used in our model product equation.

The total enzyme released from the cells does not appear as free enzyme in the fermentation broth, because significant amounts adsorb on the cellulose as we verify with our data of Figure 25. We fit the adsorption characteristics of this cellulase/cellulose system to Langmuir adsorption isotherm:

$$[A] = \frac{[A]_{max} K_{ad} [E]}{1 + K_{ad}[E]} \tag{23}$$

where A_{max} and K_{ad} are the maximum activity of enzyme adsorbed per unit weight of cellulose and the adsorption equilibrium constant, respectively. With a correlation factor R=0.95, the evaluated values of the constants were: A_{max} = 18.8 IFPU/g cellulose and K_{ad} = 2.67 ml/IFPU. This adsorption isotherm is also plotted with the original data in Figure 25.

We note use here of enzyme activity, rather than protein concentration. This convention is valid if the solution protein concentration is proportional to cellulase activity, an assumption confirmed by Ooshima et al. (1990), who examined separately the adsorption characteristics of the individual cellulase enzymes (endoglucanase, exoglucanase and *beta*-glucosidase) in connection with their activities.

With the broth enzyme activity determination assay, we were measuring only the free (not adsorbed) enzyme concentration E_f of the fermentation. Knowing the enzyme adsorption characteristics, the total enzyme activity E_t can be calculated as:

$$E_t = E_f + E_{ad} = E_f + \frac{S}{10^3} \frac{A_{max} K_{ad} E_f}{1 + K_{ad} E_f} \tag{24}$$

where E_f is free cellulase enzyme activity and E_{ad} is activity of the adsorbed cellulase enzyme.

The rate of active enzyme secretion is related to the secondary cell concentration and enzyme deactivation rate:

$$\frac{dE_t}{dt} = k_2 X_s - k_3 E_t \tag{25}$$

where k_2 is enzyme synthesis rate constant and k_3 is an enzyme decay rate constant.

3.5.5 Substrate Utilization

As noted earlier, we observed a decline of substrate reactivity with increased conversion with the cellulose fermentation (see Figure 26).

This phenomena was studied quantitatively by South (1994), who described the conversion dependence of the cellulose hydrolysis rate r to have the form:

$$r = [k_4(1-x)^{k_5} + k_6]\frac{[ES]}{A_{max}} \tag{26}$$

where x is the cellulose conversion = 1 - $\frac{\text{remaining cellulose}}{\text{initial cellulose}}$, k_4 is the hydrolysis rate constant, k_5 is the exponent of the declining substrate reactivity, k_6 is the conversion independent component in rate function and ES is the concentration of cellulose-cellulase complex.

Inserting the adsorption model (equation 23) into the rate equation (26) gives the final form of the substrate utilization rate:

$$-\frac{dS}{dt} = [k_4(1-x)^{k_5} + k_6]\frac{SK_{ad}E_f}{1 + K_{ad}E_f} \tag{27}$$

The model parameters are expected to vary for different cellulose substrates and different fermentation conditions.

3.5.6 Model Solution

The proposed set of model equations (20-22), (24-25) and (27), contain a number of parameters. We have not tried separate experimental evaluation of each parameter. A non-linear parameter estimation method was used instead for the simultaneous determination of all parameters from all substrate, biomass and product data of each batch run.

For this purpose, a Simusolv (Version 3.0) computer software package by Dow Chemical Company was used, especially designed for mathematical models of dynamic physical systems. This package executes integration of the model and compares results with the experimental data, which provides opportunity for parameter evaluation through a Method of Maximum Likelihood best fitting. The resulting parameter values and their standard deviations, calculated for five different fermentation data sets, are shown in Table 1.

The parameter values fitted to individual runs 1-5 are confined to narrow variations, i.e., similar values suffice to describe all five fermentations. The saturation parameter values of K_s = 3.6-5.5 g/L mean that above about $3K_s \approx$ 12-17 g/L, the mycelial growth rate is approximately zero order. The very small deactivation rate constant $k_3 \approx 0.01$ d^{-1} indicates on apparent enzyme half life of $t_{1/2} \approx \ln 2/k_3 > 70$ days, so over the 10 day fermentation,

deactivation is unimportant. The appreciable values of k_5, the exponential dependence of cellulose reactivity on the function (1-x) = S/S_o, validates the assumption that variable substrate reactivity requires inclusion in the model. The corresponding k_4, k_5, and k_6 values repeated by South (1994) for a substrate of lignocellulosic feedstock were $k_4 = 2.86\ h^{-1}$, $k_5 = 5.30\ h^{-1}$, and $k_6 = 0.18\ h^{-1}$.

Table 1. Parameter values and standard deviations estimated using Simusolv program

Parameter	Run 1	Run 2	Run 3	Run 4	Run 5
μ_{max}	3.0±0.29	2.4±0.23	1.6±0.26	1.7±0.25	2.3±0.26
K_s	5.5±2.3	5.2±3.5	4.0±1.7	4.9±2.1	3.6±5.6
k_1	2.4±0.39	2.1±0.65	1.5±0.36	1.6±0.33	2.2±0.41
k_d	0.16±0.03	0.12±0.02	0.09±0.07	0.09±0.05	0.09±0.05
k_2	52.4±5.1	22.7±1.8	16.2±2.1	23.0±4.2	19.8±1.4
k_3	0.0098±0.0012	0.0084±0.0070	0.0090±0.0070	0.00±0.0930	0.0092±0.0141
k_4	19.2±9.5	19.2±11.0	19.4±7.2	14.0±9.9	22.0±13.7
k_5	4.8±2.8	4.8±3.8	4.3±1.0	8.2±2.7	7.5±2.6
k_6	1.8±0.21	1.5±0.16	0.67±0.12	0.89±0.14	0.93±0.10

3.5.7 Model Fit

The model fit is shown for several cellulase fermentations performed in the same reactor system, but with different fermentation conditions (550 rpm (Figure 27), 400 rpm (Figure 28), and 250 rpm (Figures 29-31)). The graphs show that the model fits the experimental data well. However, the model equations for biomass synthesis does not predict the bimodal biomass curve seen in the data at the lowest rpm (250), a prediction which cannot be expected from equations (20-22).

3.5.8 Model Simulations

The predicted concentrations of individual primary and secondary mycelia during the course of fermentation are of interest. Model simulations for growth of primary and secondary mycelia (Run 2) with different initial substrate concentration during time course of fermentation are shown in Figure 32 and 33.

The experimental results at lower rpm (250) shows two peaks in the mycelium growth, which we rationalize as due to intensive growth of the primary mycelium (first peak) and growth of the secondary mycelium (second peak), respectively. The model predicts appreciably biomass peaks for the individual mycelial forms, but not their sum.

3.6 Conclusions

A complete batch kinetic model encompassing biomass, cellulose substrate and product cellulase has been constructed and shown to fit five sets of batch data reasonably well. Known biological and biochemical features incorporated in the model include:

1. structured biomass (primary and secondary mycelia)
2. secondary mycelia are sole producers of cellulases
3. enzyme adsorption equilibrium between cellulose and bulk solution.
4. continuous decline of substrate reactivity with cellulose conversion.

4 Overall Conclusions and Recommendations

In batch fermentations, *Trichoderma reesei* biomass–concentration profiles exhibited either unimodal or bimodal behavior versus time, depending on the substrate (soluble xylose or particulate solid cellulose). When *T. reesei* are grown on cellulose (Solka Floc), a rapid initial biomass growth occurs, apparently due to availability of yeast extract in the growth medium. Later, when sufficient cellulase is present, the cellulose hydrolysis rate rises substantially to support a second growth phase on the more recalcitrant, cellulose fraction of the growth medium. The second growth phase halts when cellulose is consumed.

Cells grown at 250 rpm, and sparged with air only were oxygen limited, and showed low biomass concentration and final cellulase activity, when compared with cells grown in oxygen supplemented air. The critical dissolved oxygen (DO) concentration, C_{crit}, was determined to be 0.073 mmol O_2/L. The broth DO was maintained above this level to prevent oxygen limitations.

A kinetic model for batch production of cellulase enzyme by *T. reesei* grown on cellulose nutrient was constructed, and includes the following four assumptions: (1) Fungal cells exist in one of two forms, termed primary or secondary, that appear at different times in batch fermentations. (2) Only secondary mycelia, found in the second growth stage, produce cellulase enzyme activity. (3) Cellulase enzymes strongly adsorb on the cellulose nutrient, according to Langmuir adsorption kinetics. (4) Cellulose reactivity declines with increased conversion. Model fits for fermentations at 250, 400 and 550 rpm show good agreement with the experimental data.

In all fermentations, the Casson model best fit steady shear rheological data, and thus Casson parameters of yield stress and Casson viscosity were used to describe the rheological behavior of the cell broth. In all cellulose fermentations, there was a strong correlation between Casson model parameters and cell–mass concentration during the first growth stage. Then, as biomass concentration declined somewhat in the latter half of the fermentation, the yield stress and the Casson viscosity declined more strongly and the correlation between cell mass and Casson parameters disappeared. Microscopy revealed that cellular morphology had changed significantly, resulting in microstructural breakdown in the broth, and causing substantial decreases in both yield stress and Casson viscosity.

Dynamic, oscillatory shear measurements showed consistent, low-strain "gel-like" behavior and high-strain "liquid-like" behavior for all suspensions, independent of concentration and time. This implies there could be substantial absence of mixing in large scale *T. reesei* fermentations in regions of low shear. The low strain, time-dependent variation of both the elastic (G') and viscous (G") moduli were similar to the bimodal trends found for Casson model parameters, corroborating the steady shear rheological data.

Mycelial morphology, and probably cell lysis, play key roles in broth rheological be-

havior. Further studies to quantitate morphology and lysis would allow development of correlations for prediction of apparent viscosity as a function of biomass and morphology, and thus of time. This information could then be used to predict the oxygen mass transfer coefficient as a function of time, and a full reactor design model including mixing, mass transfer, and cellulase production would be available.

We showed in Chapter 2, that there were no completely-stagnant regions in the fermentor during our fermentations. This however, does not imply that the contents of the fermentor were perfectly mixed. Mixing studies which seek optimal impeller configurations would allow quantitative determination of mixing times and power consumption requirements, and provide maintenance of sufficiently high oxygen mass transfer coefficients and shear rates below those which produce cell damage.

5 References

Allen, D. and Robinson, C. (1990). Measurement of rheological properties of filamentous fermentation broths. *Chem. Eng. Sci.*, 45:37–48.

Ang, J. (1991). Water retention capacity and viscosity effect of powdered cellulose. *J. Food Sci.*, 56:1682–1684.

Aranguren, M., Mora, E., DeGroot, J., and Macosko, C. (1992). Effect of reinforcing fillers on the rheology of polymer melts. *J. Rheology*, 36:1165–1182.

Bader, J., Klingspohn, U., Bellgardt, K., and Schugerl, K. (1993). Modeling and simulation of the growth and enzyme production of *trichoderma reesei* rut c30. *J. Biotechnol.*, 29:121–135.

Bird, R., Armstrong, R., and Hassager, O. (1987). *Dynamics of Polymeric Liquids, Vol 1: Fluid Mechanics, 2nd ed.* Wiley, New York.

Bongenaar, J., Kossen, N., Metz, B., and Meijboom, F. (1973). A method for characterizing the rheological peoperties of viscous fermentation broths. *Biotechnol. Bioeng.*, 15:201–206.

Bozell, J. and Landucci, R., editors (1993). *Alternative Fedstocks Porgram Technical and Economic Assessment: Thermal/Chemical and Bioprocessing Components.* U.S. Department of Energy Office of Industrial Technologies.

Brown, D. and Halsted, D. (1975). The effect of acid ph on the growth kinetics of *trichoderma viride. Biotechnol. Bioeng.*, 17:11.

Brown, D. and Zainudeen, M. (1977). Growth kinetics and cellulase biosynthesis in the continuous culture of *trichoderma viride. Biotechnol. Bioeng.*, 19:941–958.

Chan, E. (1985). Studies in flocculated polymer/particle dispersions. *Ph.D. Thesis, Princeton University.*

Chanal, P., Chanal, D., and Andre, G. (1992). Cellulase production profile of *trichoderma reesei* on different cellulosic substrates at various ph levels. *J. Ferment. Bioeng.*, 74:126–128.

Charles, M. (1978). Technical aspects of the rheological properties of microbial cultures. *Adv. Biochem. Eng.*, 8:1–62.

Chmiel, H., Krischke, W., Schmid, U., Schuttoff, M., Walitza, E., and Wessling, V. (1990). Rheology and mass transfer in mycelial fermentation broth. In Oliver, D., editor, *3rd European Rheology Conference and Golden Jubilee Meeting of the Brithish Society of Rheology*, pages 104–106. Elsevier Applied Science, London.

Doskocil, J., Sikyta, B., Kasparova, J., Doskocilova, D., and Zajfcek, J. (1958). Development of the culture of streptomyces rimosus in submerged fermentation. *J. Gen. Microbiol.*, 18:302–314.

Elson, T. (1988). Mixing of fluids possessing a yield stress. *Proc. 6th European Conf. on Mixing, Pavia, Italy, Organized by AIDIC -Associazione Italiana di Ingegeneria Chemica*, pages 485–492.

Elson, T. (1990). The growth of caverns formed around rotating impellers during the mixing of a yield stress fluid. *Chem. Eng. Comm.*, 96:303–319.

Ferry, J. (1980). *Viscoelastic Properties of Polymers, 3rd edition.* John Wiley and Sons, New York.

Gaden, E. (1955). Fermentation kinetics and productivity. *Chem. Ind.*, pages 154–159.

Galindo, E., Nienow, A., and Badham, R. (1988). Mixing of simulated xanthan gum broths. In King, R., editor, *2nd International Conference on Bioreactor Fluid Dynamics*, pages 65–78. Elsevier on behalf of BHRA, London.

Ghose, T. (1987). Measurement of cellulase activities. *Pure Appl. Chem.*, 59:257–268.

Ghose, T. and Sahai, V. (1979). Production of cellulases by *trichoderma reesei* qm 9414 in fed-batch and continuous-flow culture with cell recycle. *Biotechnol. Bioeng.*, 21:283–296.

Graessley, W. (1993). Viscoelasticity and flow in polymer melts and concentrated solutions. In Mark, J., Eisenberg, A., Graessley, W., Mandelkern, L., Samulski, E., Koenig, J., and Wignall, G., editors, *Physical Properties of Polymers, Second Edition*, pages 97–143. Americal Chemical Society, Washington, D.C.

Hendy, N., Wilke, C., and Blanch, H. (1982). Enhanced cellulase production using Solka Floc in a fed-batch fermentation. *Biotech. Let.*, 4:785–788.

Kemblowski, Z. and Kristiansen, B. (1986). Rheometry of fermentation liquids. *Biotechnol. Bioeng.*, 28:1474–1483.

Khan, S., Baker, G., and Colson, S. (1994). Composite polymer electrolytes using fumed silica fillers: Rheology and ionic conductivity. *Chem. Mater.*, 6:2359–2363.

Khan, S. and Zoeller, N. (1993). Dynamic rheological behavior of flocculated fumed silica suspensions. *J. Rheol.*, 37:1225–1235.

Kilpatrick, P., Khan, S., Tayal, A., and Blackburn, J. (1994). Rheological study of polycrystalline lyotropic mesophases in the cesium n-tetradecanoate–water system. In Herb, C. and Prud'homme, R., editors, *Structure and Flow in Surfactant Solutions*, pages 229–238. American Chemical Society, Washington, D.C.

Kim, D., Kim, T., Jeong, Y., and Lee, J. (1992). Adsorption kinetics and behaviors of cellulase components on microcrystaline cellulose. *J. Ferment. Bioeng.*, 73:461–466.

Klingspohn, U. (1990). Verfahrenstechnische aspekte der produktion und aufarbeitung von enzymen zur nutzung nachwachsender rohstoffe. *Dissertation, Univ. Hanover.*

Leong-Poi, L. and Allen, D. (1992). Direct measurement of the yield stress of filamentous fermentation broths with the rotating vane technique. *Biotechnol. Bioeng.*, 40:403–412.

Marten, M., Velkovska, S., Khan, S., and Ollis, D. (May, 1994). Rheological characterization of cellulase-producing fungal suspensions. *Sixteenth Symposium on Biotechnology for Fuels and Chemicals*, pages Gatlinburg, TN.

Matsumura, M., Imanaka, T., and Yoshida, T. (1981). Modeling of cephalosporin c production and its application to fed-batch culture. *J. Ferment. Technol.*, 59:115–123.

Metz, B., Kossen, W., and van Suijdam, J. (1979). The rheology of mould suspensions. *Adv. Biochem. Eng.*, 11:103–156.

Metzner, A. and Otto, R. (1957). Agitation of non-Newotnian fluids. *AICHE J.*, 3:3–10.

Mitra, G. and Wilke, C. (1975). Continuous cellulase production. *Biotechnol. Bioeng.*, 17:1–13.

Mohagheghi, A. (1993). Personal communication.

Mohagheghi, A., Grohmann, K., and Wyman, C. (1988). Production of cellulase on mixtures of xylose and cellulose. *Appl. Biochem. Biotech*, 17:263–277.

Mohagheghi, A., Grohmann, K., and Wyman, C. (1990). Production of cellulase on mixtures of xylose and cellulose in a fed-batch process. *Biotechnol. Bioeng.*, 35:211–216.

Nienow, A. and Elson, T. (1988). Aspects of mixing rheologically complex fluids. *Chem. Eng. Res. Des.*, 66:5–15.

Nutor, J. and Converse, A. (1991). The effect of enzyme and substrate levels on the specific hydrolysis rate of pretreated poplar wood. *Appl. Biochem. Biotechnol.*, 28/29:757–772.

Obraztsova, I., Rabinovich, M., and Fedosenko, M. (1993). Kinetics of enzymatic cellulose hydrolysis and possible use in process acceleration. *Prikladn. Biokhim. Mikrobiol.*, 29:684–689.

Olsvik, E., Tucker, K., Thomas, C., and Kristiansen, B. (1993). Correlation of *Aspergillus niger* broth rheological properties with biomass concentration and the shape of mycelial aggregates. *Biotechnol. Bioeng.*, 42:1046–1052.

Oolman, T. and Blanch, H. (1986). Non-Newtonian fermentation systems. *CRC Critical Reviews in Biotechnology*, 4:133–185.

Oolman, T., Walitza, E., Hanssmann, E., and Chmiel, H. (1987). Viscoelasticity and mass transfer in bioreactors. In Chmiel, H., Hammes, W., and Bailey, J., editors, *Biochemical Engineering a Challenge for Interdisciplinary Cooperation*, pages 416–420. Gustav Fischer Verlag, Stuttgart.

Oosima, H., Burns, D., and Converse, A. (1990). Adsorption of cellulase from *trichoderma reesei* on cellulose and lignacious residue in wood pretreated by dilute sulfuric acid with exlosive decompression. *Biotechnol. Bioeng.*, 36:446–452.

Rakshit, S. and Sahai, V. (1991). Optimal control strategy for the enhanced production of cellulase enzyme using the new mutant *Trichoderma reesei* E-12. *Bioproc. Eng.*, 6:101–107.

Reuss, M., Debus, D., and Zoll, G. (1982). Rheological properties of fermentation fluids. *Chem. Eng.*, 381:233–236.

(Rodeh), R. S., Stavy, L., and Galun, E. (1970). Protein synthesis in aged and young zones of *trichoderma* colonies. *Biochim. Biophys. Acta.*, 217:468–476.

Solomon, J., Elson, T., Nienow, A., and Pace, G. (1981). Cavern sizes in agitated fluids with a yield stress. *Chem. Eng. Comm.*, 11:143–164.

South, C. (1994). Reactor design considerations for the conversion of particulate biomass to ethanol. *PhD Thesis, Dartmouth College, Hanover, NH.*

Stanbury, P. and Whitaker, A. (1984). *Principles of Fermentation Technology.* Pergamon Press, Oxford.

Sternberg, D. and Dorval, S. (1979). Cellulase production and ammonia metabolism in *trichoderma reesei* on high levels of cellulose. *Biotechnol. Bioeng.*, 21:181–191.

Tucker, K., Mohan, P., and Thomas, C. (1993). The influence of mycelial morphology on the rheology of filamentous fermentation broths. In Nienow, A., editor, *Bioreactor and Bioprocess Fluid Dynamics*, page 261. BHR Group, London.

Vallander, L. and Eriksson, K. (1985). Enzymatic saccharification of pretreated wheat straw. *Biotechnol. Bioeng.*, 27:650–659.

Velkovska, S. (1995). Kinetic models for batch fermentations for (i) itaconic acid and (ii) cellulase production. *M.S. Thesis, North Carolina State University.*

Velkovska, S., Marten, M., and Ollis, D. (1995). Kinetic model for growth and cellulase production in *Trichoderma reesei* batch fermentations. *J. Biotechnol.*, (submitted).

Wang, D., Cooney, C., Demain, A., Dunnill, P., Humphrey, A., and Lilly, M. (1979). *Fermentation and Enzyme Technology.* John Wiley and Sons, New York.

Webster, J. (1980). *Introduction to Fungi.* Cambridge University Press, New York.

Wichterle, K. and Wein, O. (1979). Threshold of mixing on non-Newtonian fluids. *Int. Chem. Engng.*, 21:116–120.

6 Figures

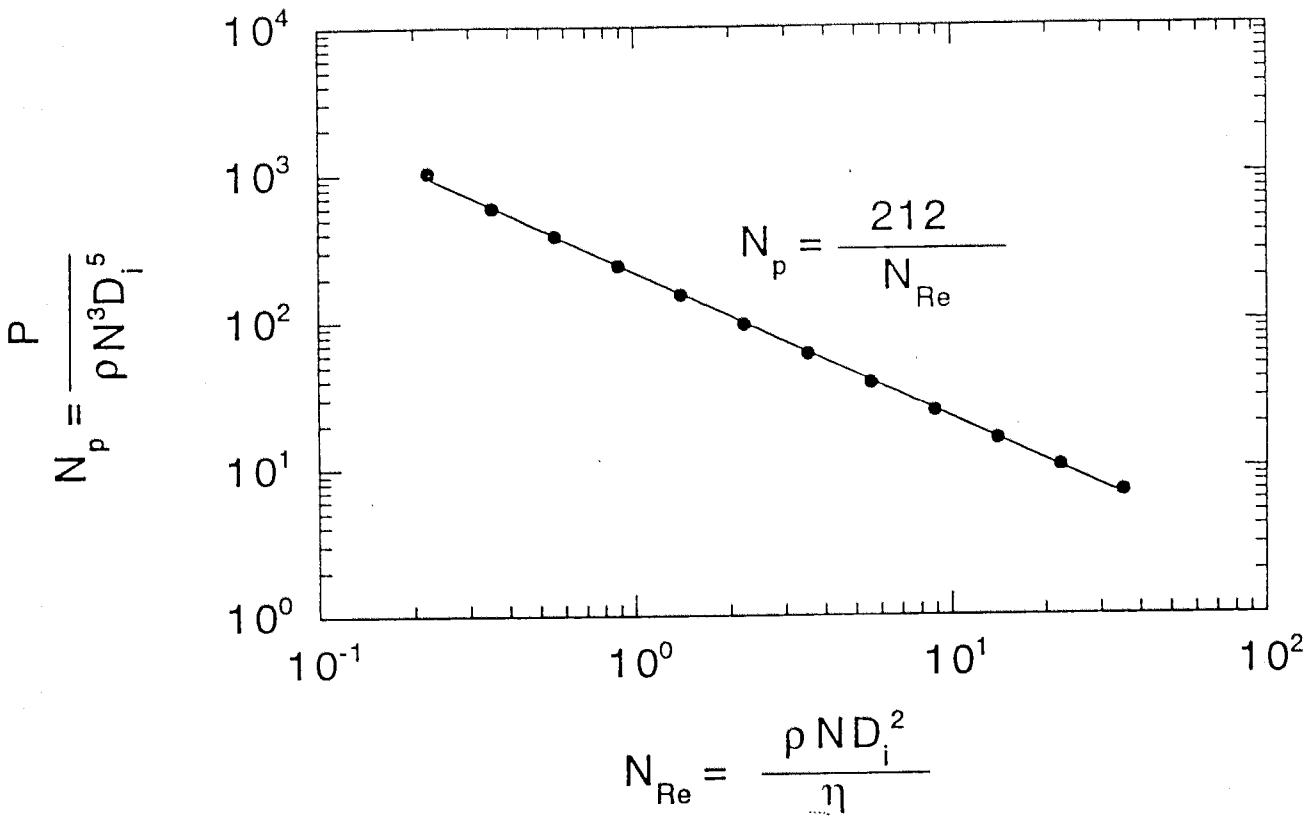

Figure 1: Power number versus Reynolds number for vane-and-cup. Laminar flow regime with silicon oil at $23°C$.

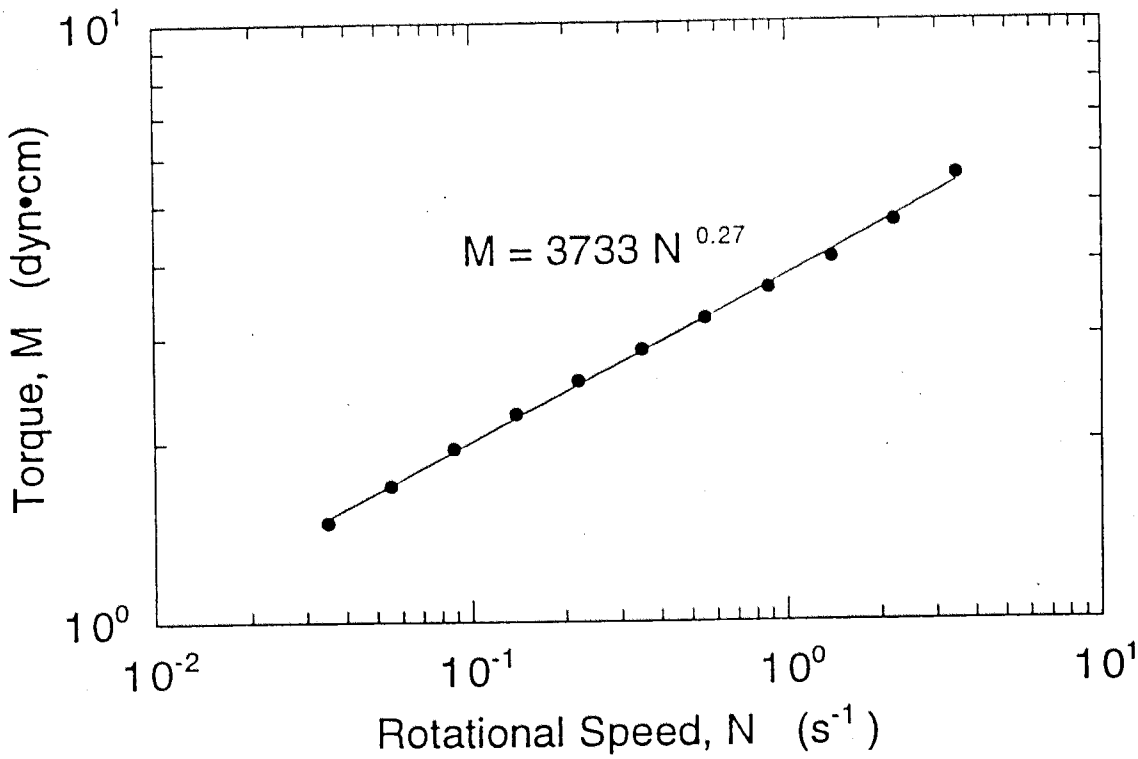

Figure 2: Torque (M) versus rotational speed (N) for 0.4(w/v)% xanthan gum in our vane-and-cup. All points shown were in the laminar flow regime.

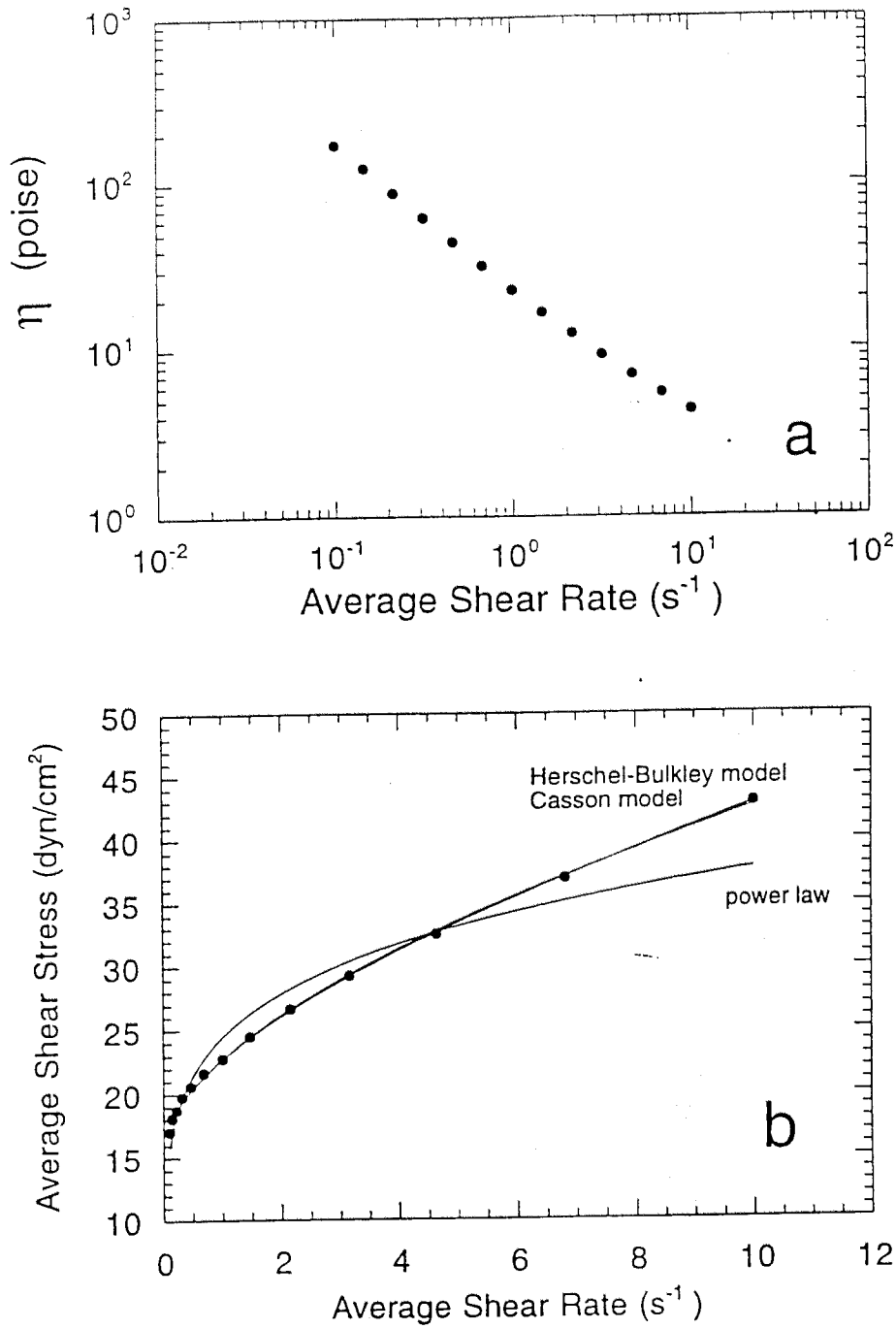

Figure 3: *T. reesei* fungal suspension grown on 5.0% initial cellulose, sample removed 1.3 days after inoculation. (a) Apparent viscosity (η) as a function of average shear rate (b) Average shear stress (τ_{avg}) versus average shear rate ($\dot{\gamma}_{avg}$), fits for power law, Casson, and Herschel-Bulkley models. Casson and Herschel-Bulkley fits overlap strongly.

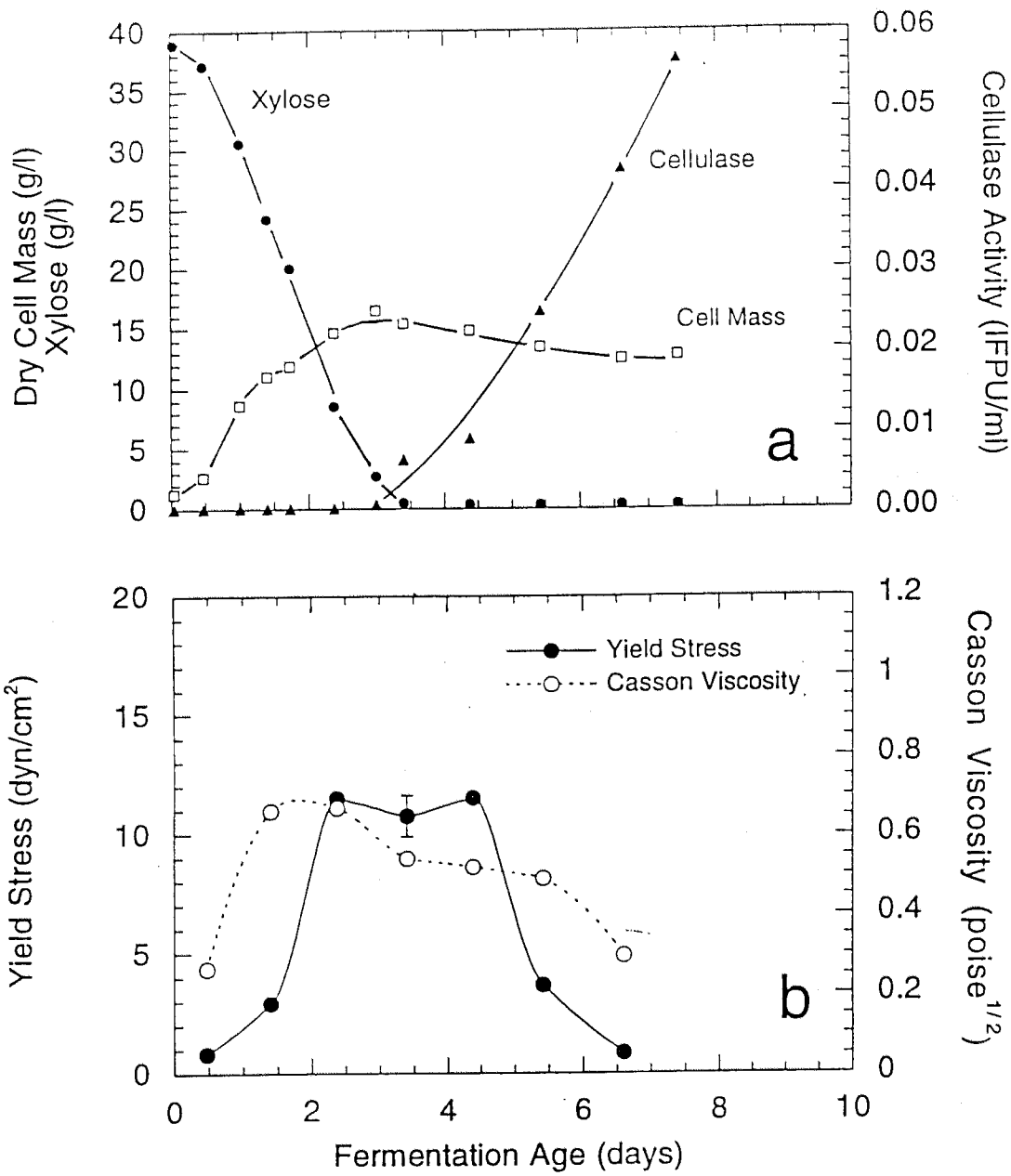

Figure 4: Profiles for *T. reesei* fungal fermentation with 4.0% initial xylose (soluble substrate). (a) Variation in dry cell mass, cellulase activity, and reducing sugar concentration. (b) Casson model parameters: yield stress (τ_y) and Casson viscosity (K_c).

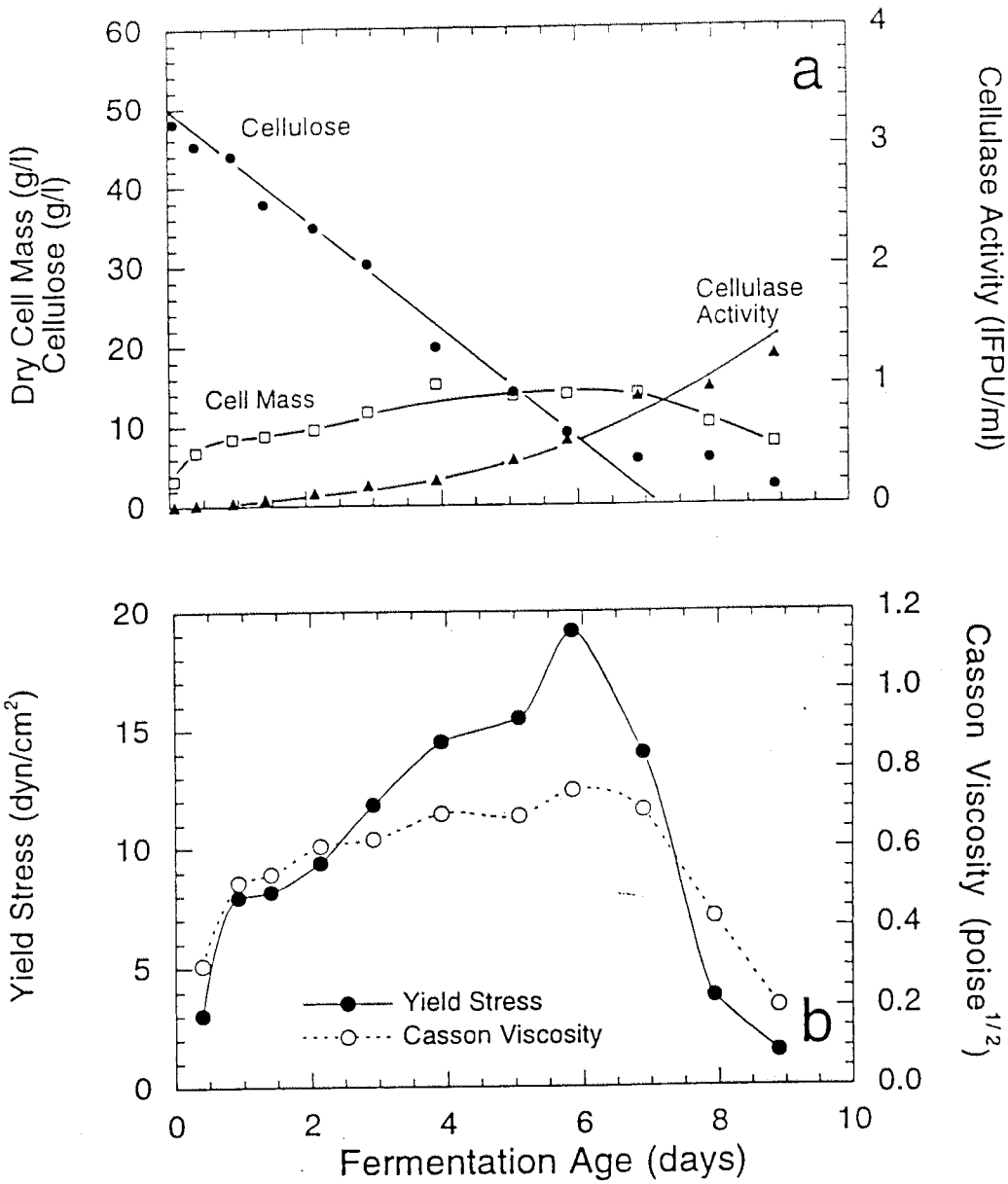

Figure 5: Profiles for a *T. reesei* fermentation sparged with air only; fermentor impeller speed, 250 rpm; initial Solka Floc, 5%. (a) Variation in dry cell mass, cellulase activity, and cellulose concentration. (b) Casson model parameters: yield stress (τ_y) and Casson viscosity (K_c).

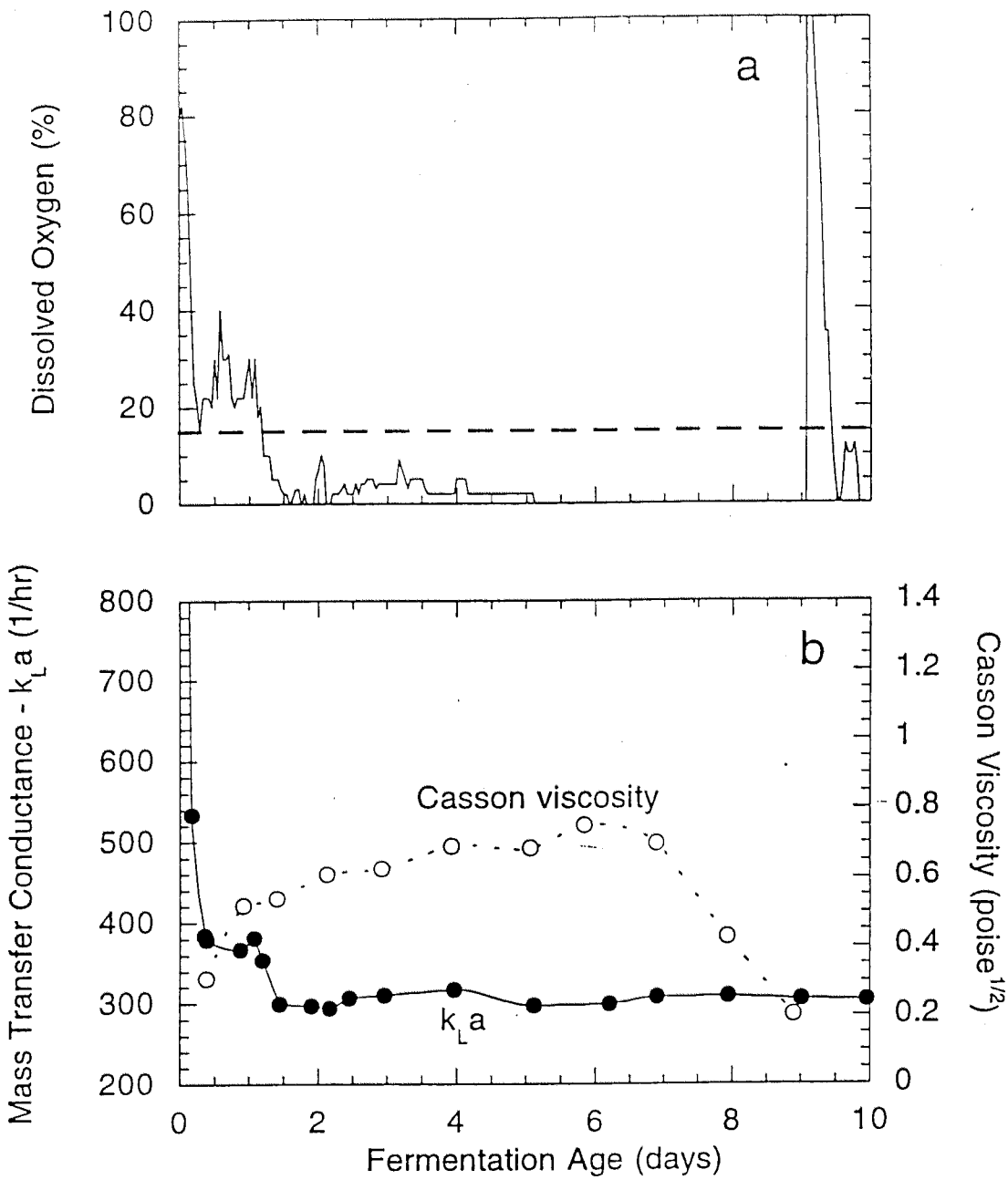

Figure 6: Data from fermentation shown in Figure 5. (a) Fermentation broth dissolved oxygen concentration. (b) Mass transfer conductance ($k_L a$) and Casson viscosity.

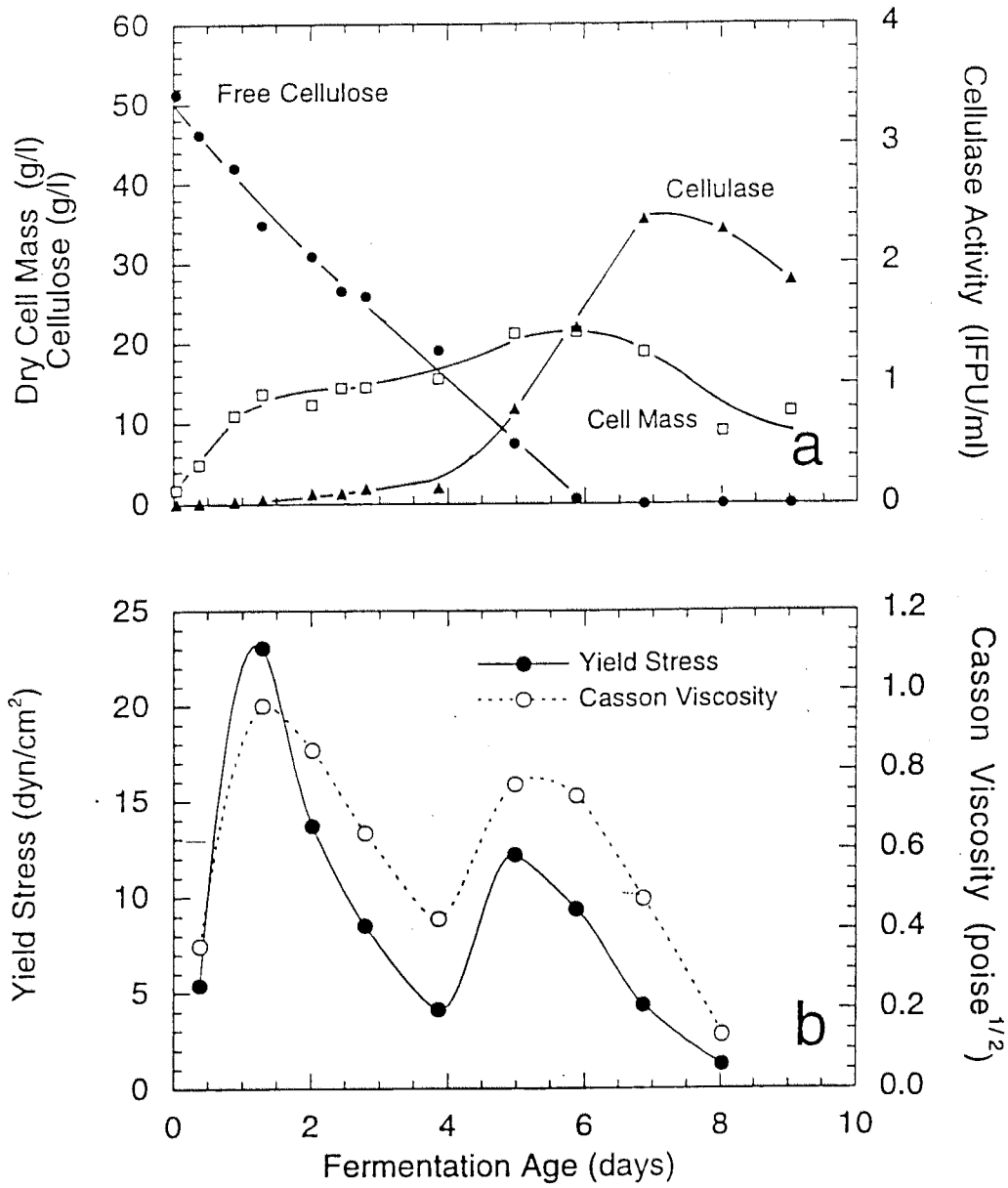

Figure 7: *T. reesei* fermentation sparged with a combination of air and pure oxygen; fermentor impeller speed, 250 rpm; initial Solka Floc, 5%. (a) Variation in dry cell mass, cellulase activity, and cellulose concentration. (b) Casson model parameters: yield stress (τ_y) and Casson viscosity (K_c).

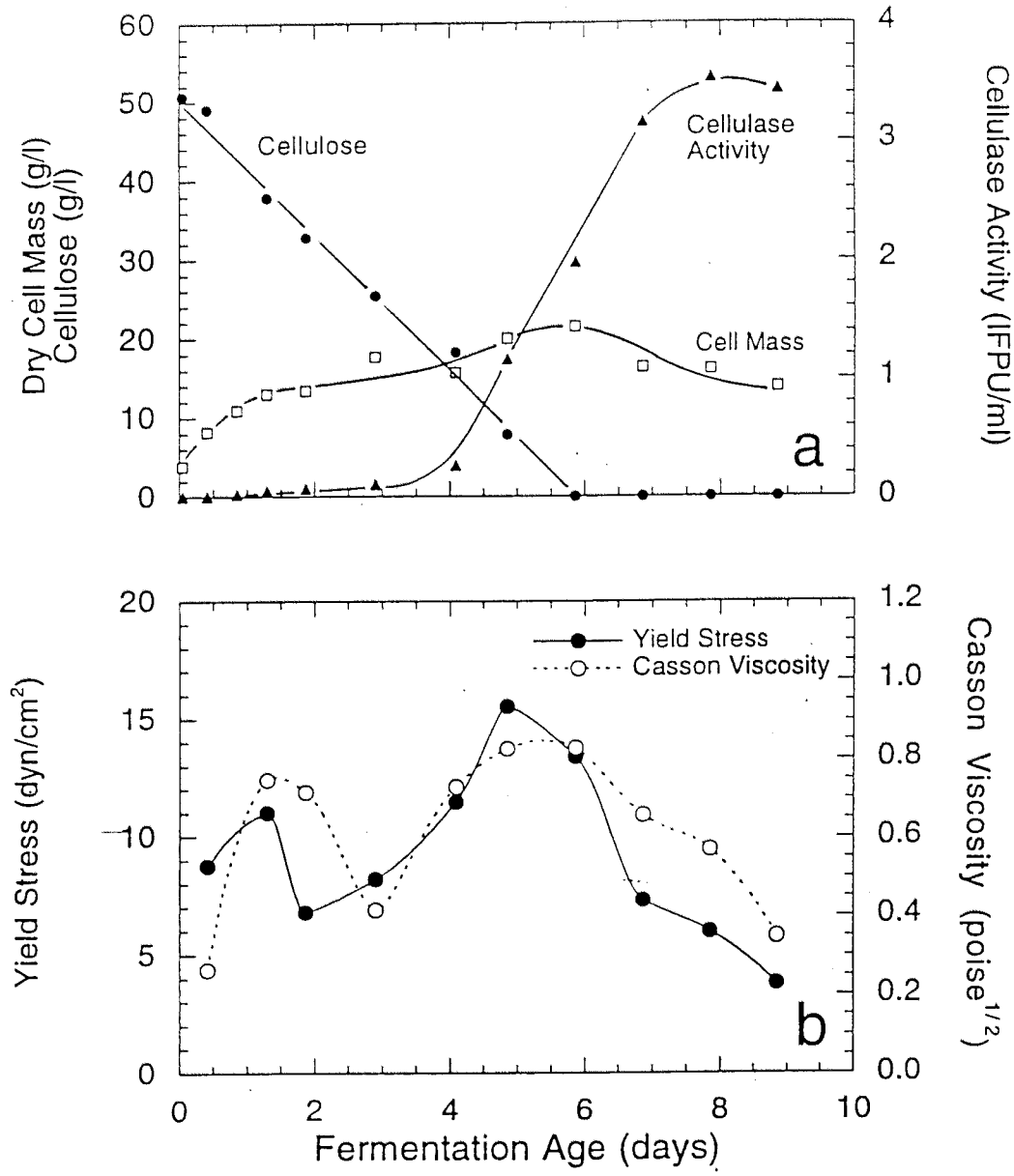

Figure 8: Fermentation identical to that shown in Figure 7. (a) Variation in dry cell mass, cellulase activity, and cellulose concentration. (b) Casson model parameters: yield stress (τ_y) and Casson viscosity (K_c).

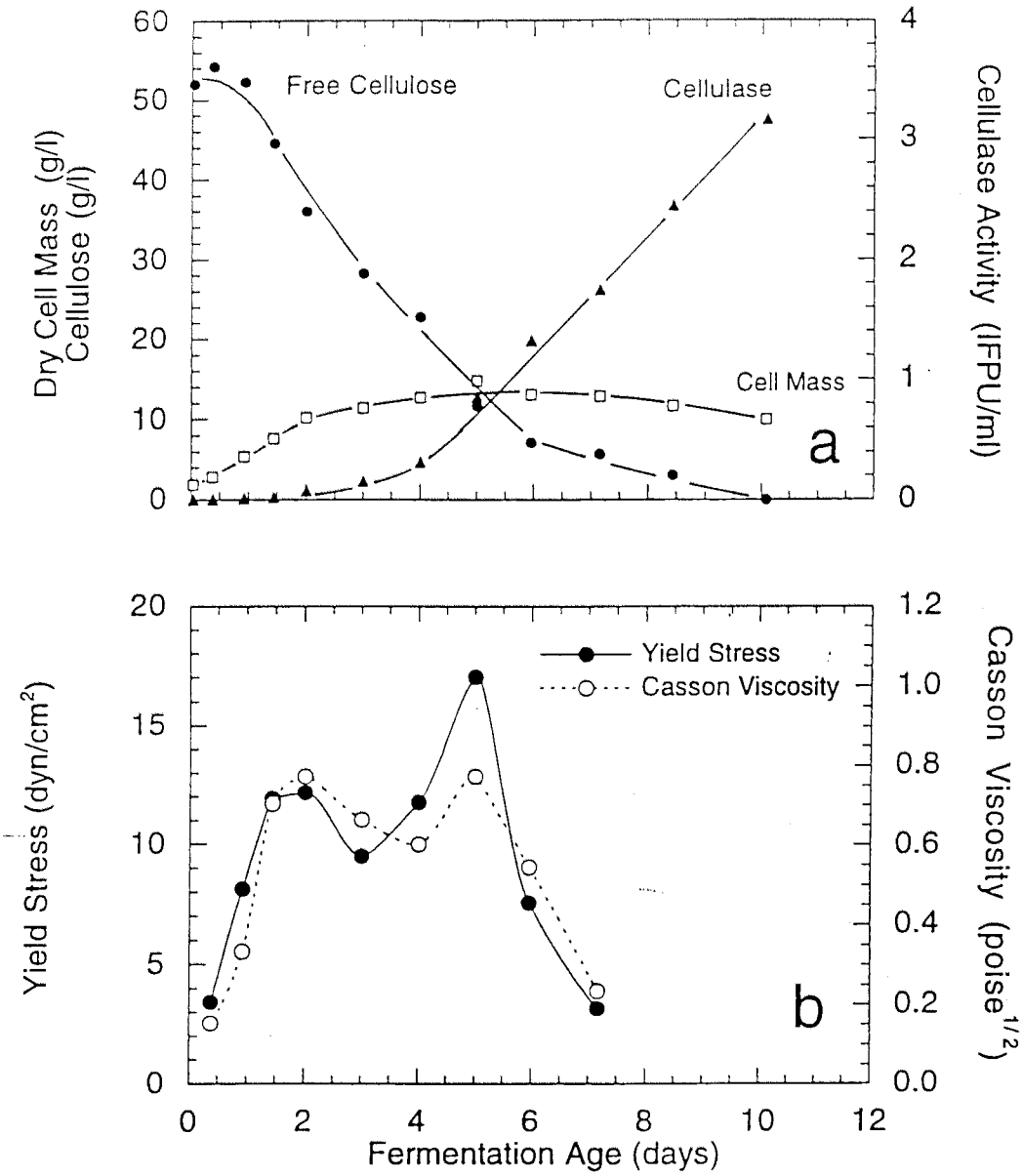

Figure 9: *T. reesei* fermentation grown on pure micro-crystalline cellulose (5% initial Sigmacell), sparged with a combination of air and pure oxygen; fermentor impeller speed, 250 rpm. (a) Variation in dry cell mass, cellulase activity, and cellulose concentration. (b) Casson model parameters: yield stress (τ_y) and Casson viscosity (K_c).

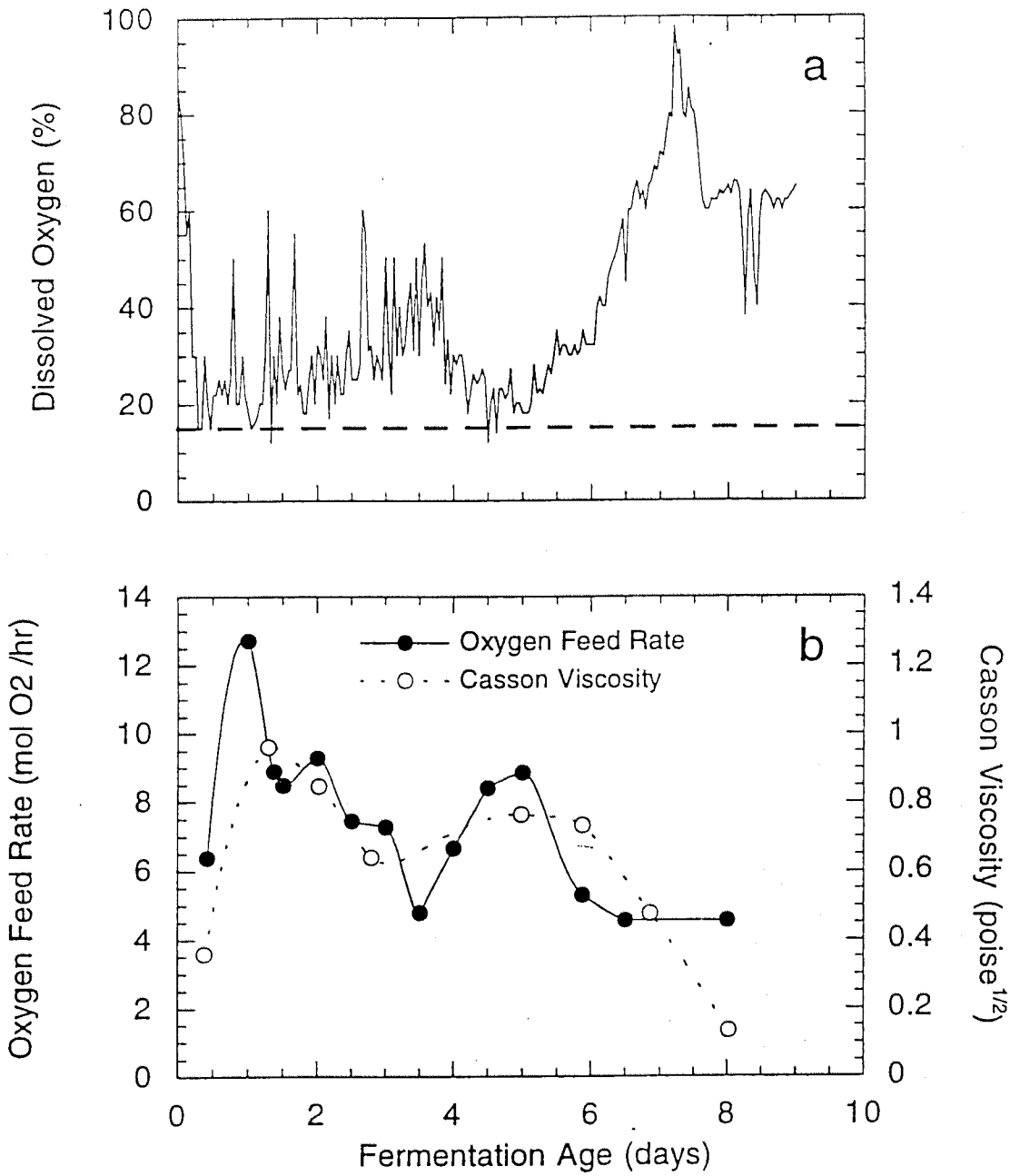

Figure 10: Data from fermentation shown in figure 7. (a) Fermentation broth dissolved oxygen concentration. (b) Mass transfer conductance ($k_L a$) and Casson viscosity.

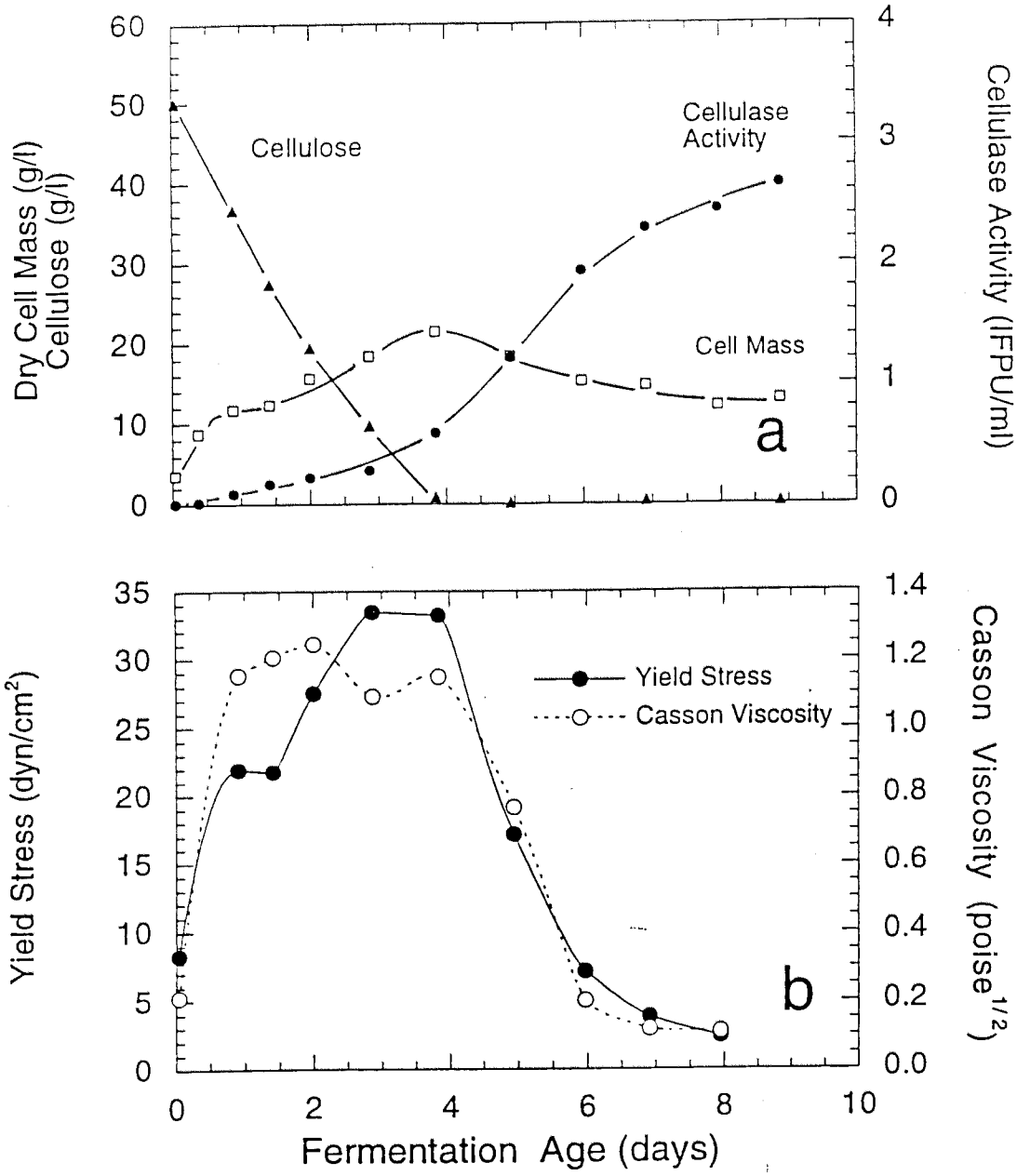

Figure 11: *T. reesei* fermentation at 400 rpm impeller speed, sparged with a combination of air and pure oxygen; initial Solka Floc, 5%. (a) Variation in dry cell mass, cellulase activity, and cellulose concentration. (b) Casson model parameters: yield stress (τ_y) and Casson viscosity (K_c).

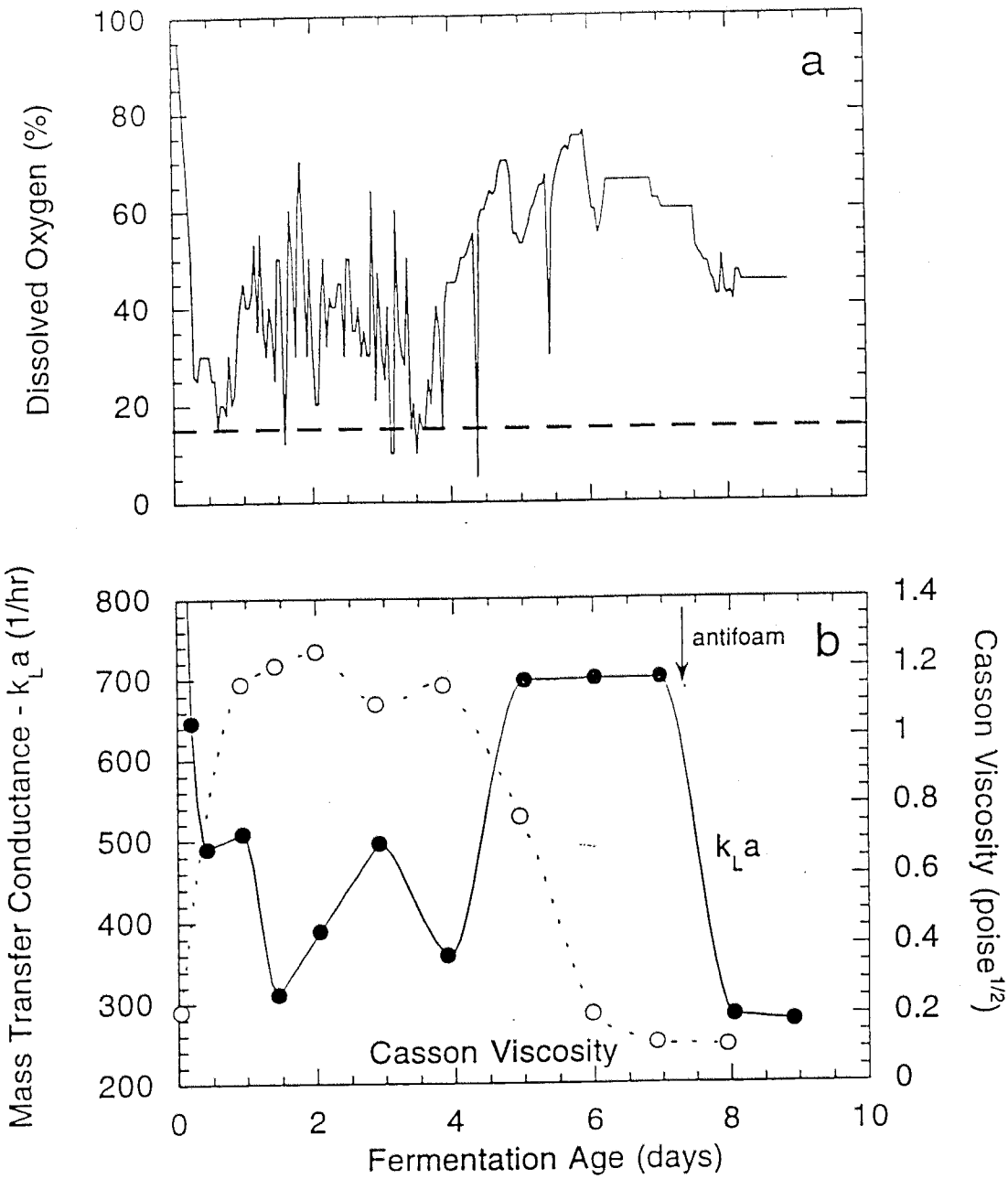

Figure 12: Data from fermentation shown in figure 11. (a) Fermentation broth dissolved oxygen concentration. (b) Mass transfer conductance (k_La) and Casson viscosity.

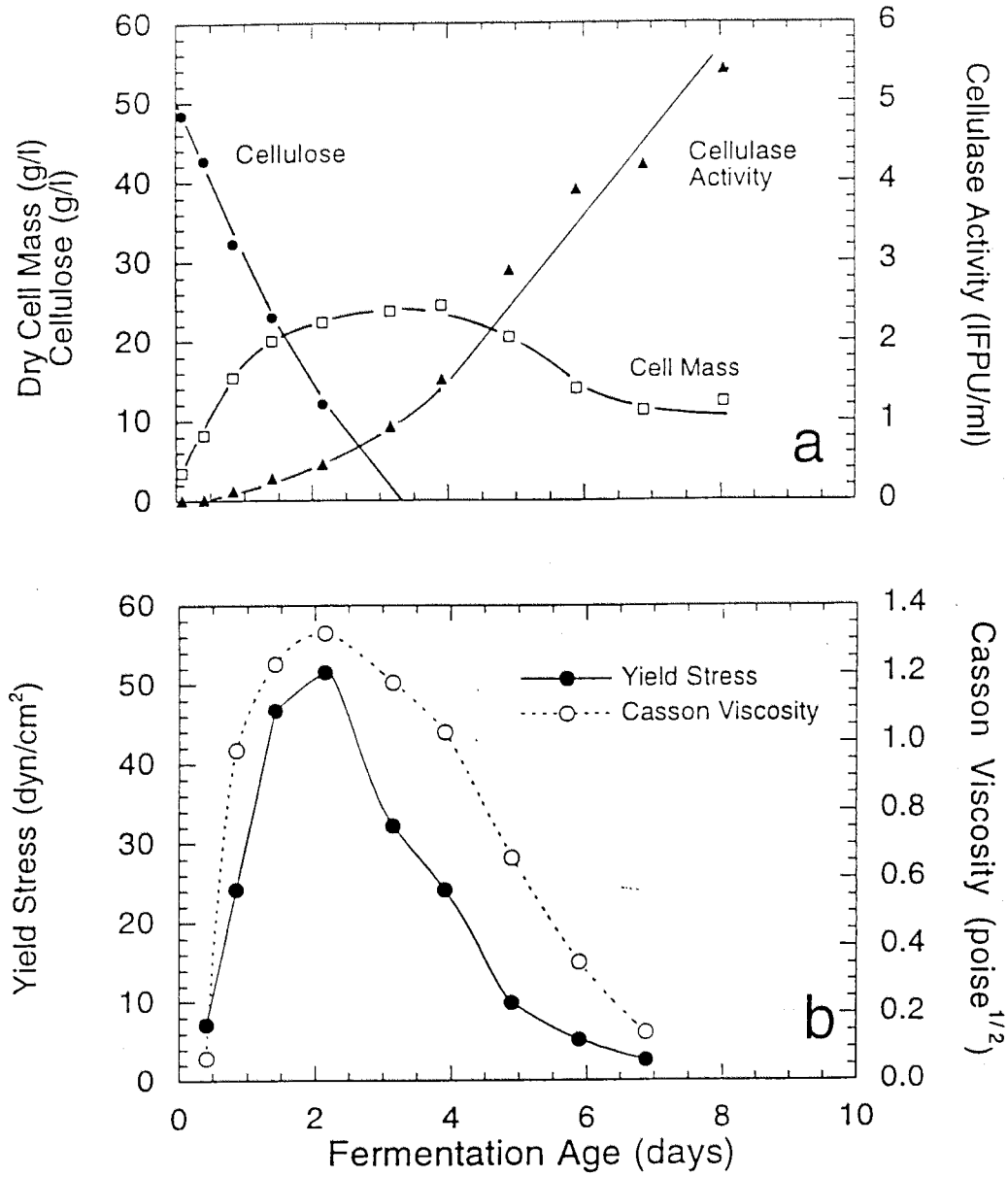

Figure 13: *T. reesei* fermentation at 550 rpm, sparged with a combination of air and pure oxygen; initial Solka Floc, 5%. (a) Variation in dry cell mass, cellulase activity, and cellulose concentration. (b) Casson model parameters: yield stress (τ_y) and Casson viscosity (K_c).

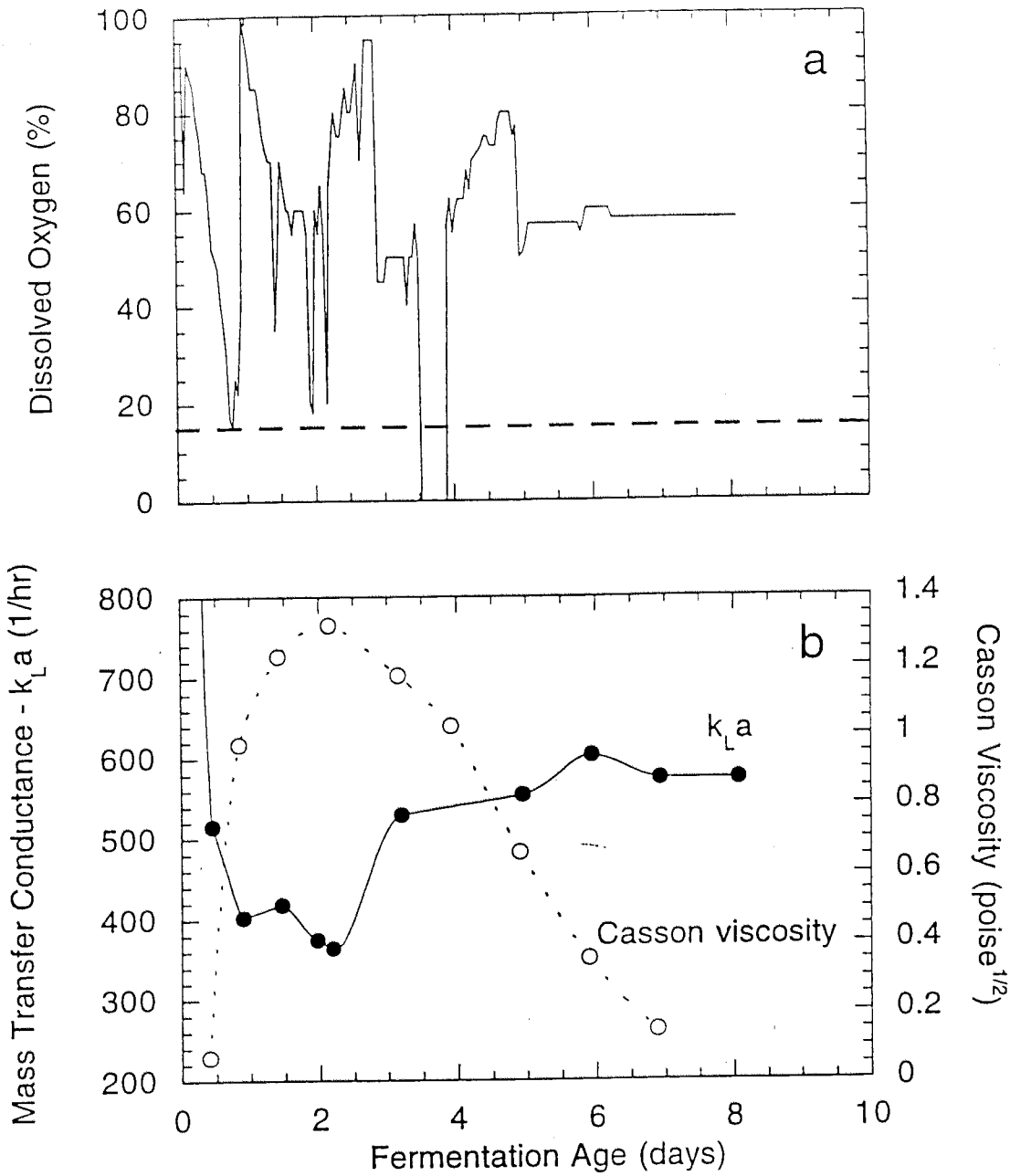

Figure 14: Data from fermentation shown in figure 13. (a) Fermentation broth dissolved oxygen concentration. (b) Mass transfer conductance ($k_L a$) and Casson viscosity.

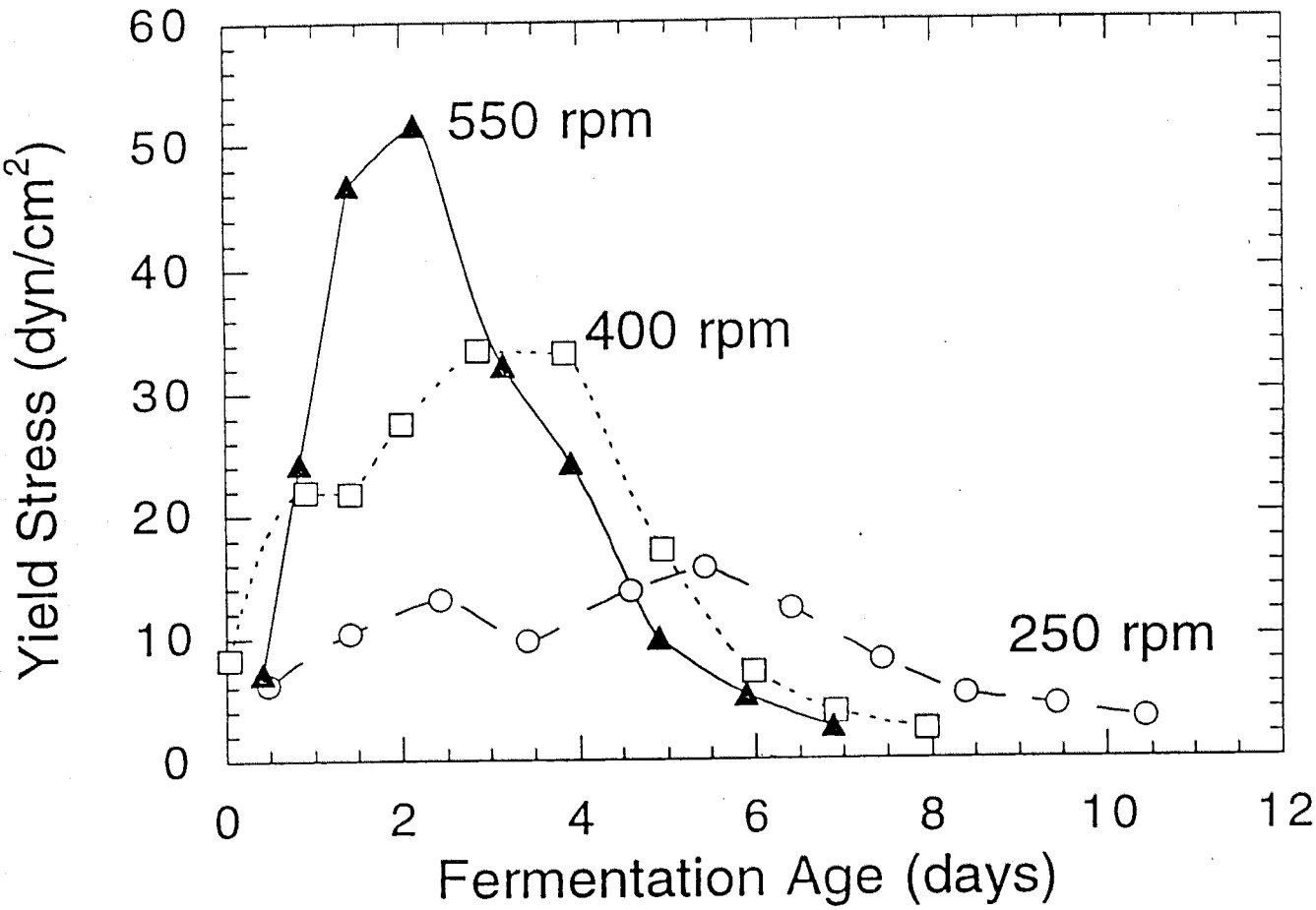

Figure 15: Variation in yield stress for *T. reesei* fermentations at three impeller speeds (250, 400, and 550 rpm).

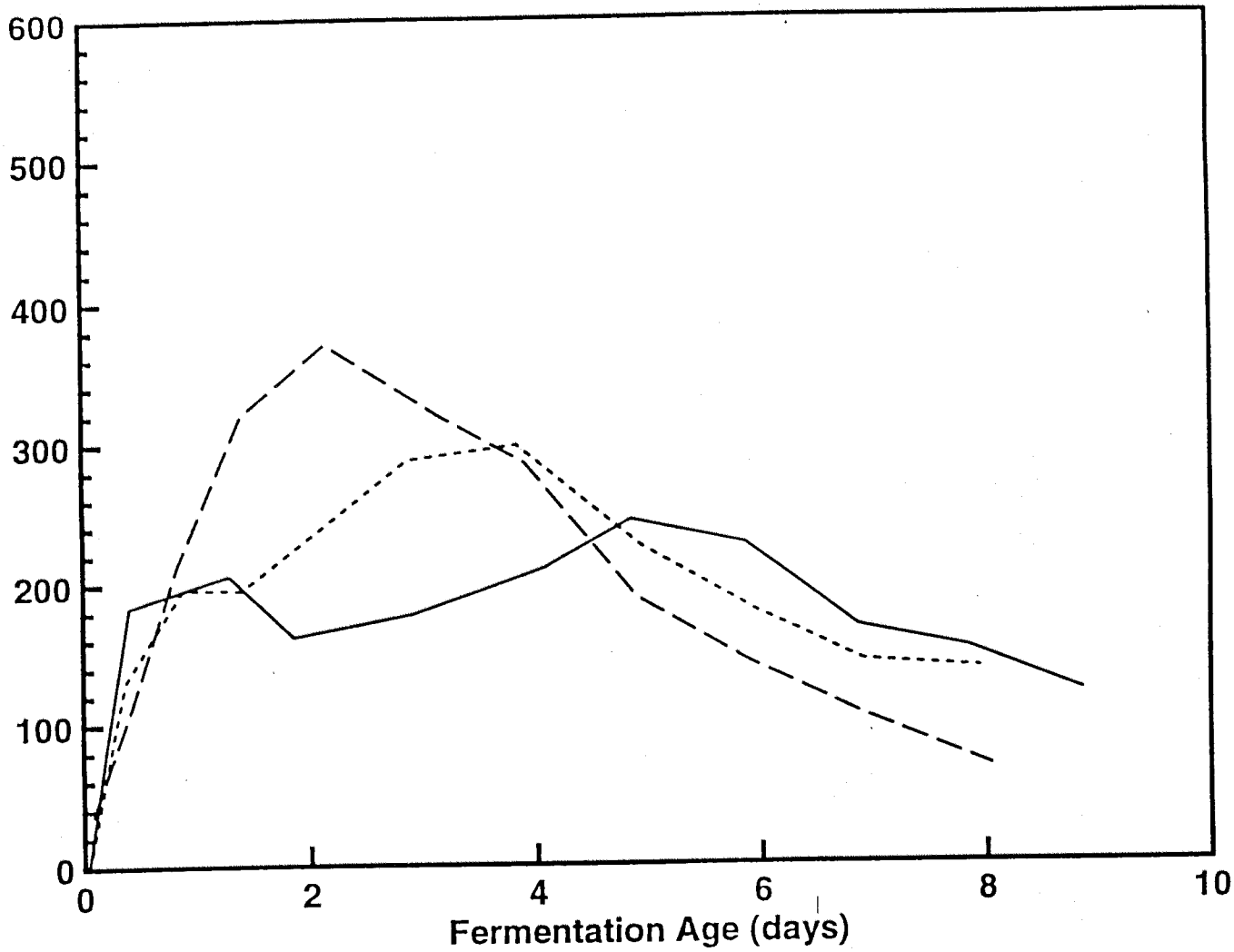

Figure 16: Rotational speed necessary for cavern diameter to reach vessel wall (N_w) for fermentations at three different impeller speeds; (———) 250 rpm, (· · · · ·) 400 rpm, (— — —) 550 rpm.

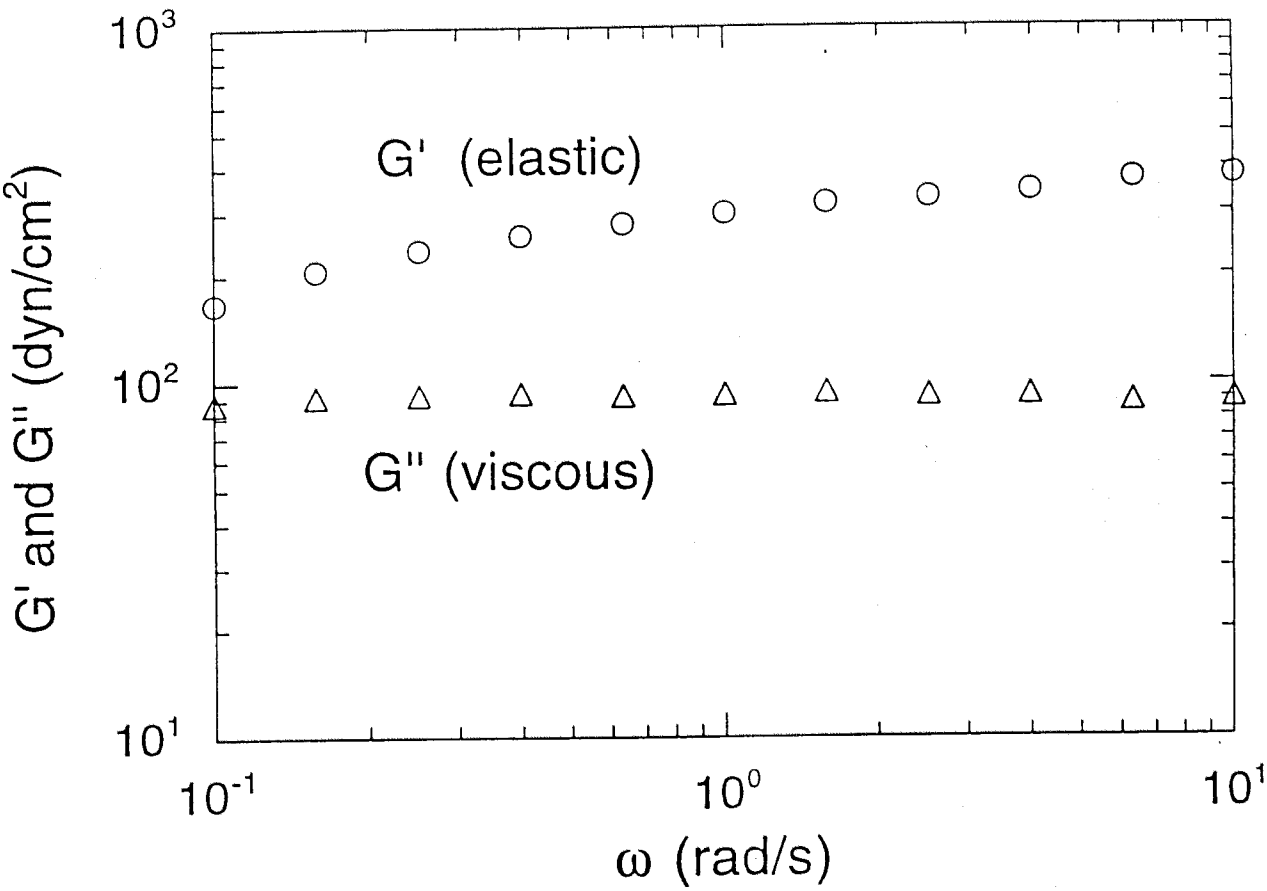

Figure 17: Dynamic moduli G' (elastic) and G" (viscous) as a function of frequency (ω), in a typical frequency sweep oscillatory strain measurement. Test sample taken from a *T. reesei* fermentation with 5% initial cellulose, 1.3 days after inoculation.

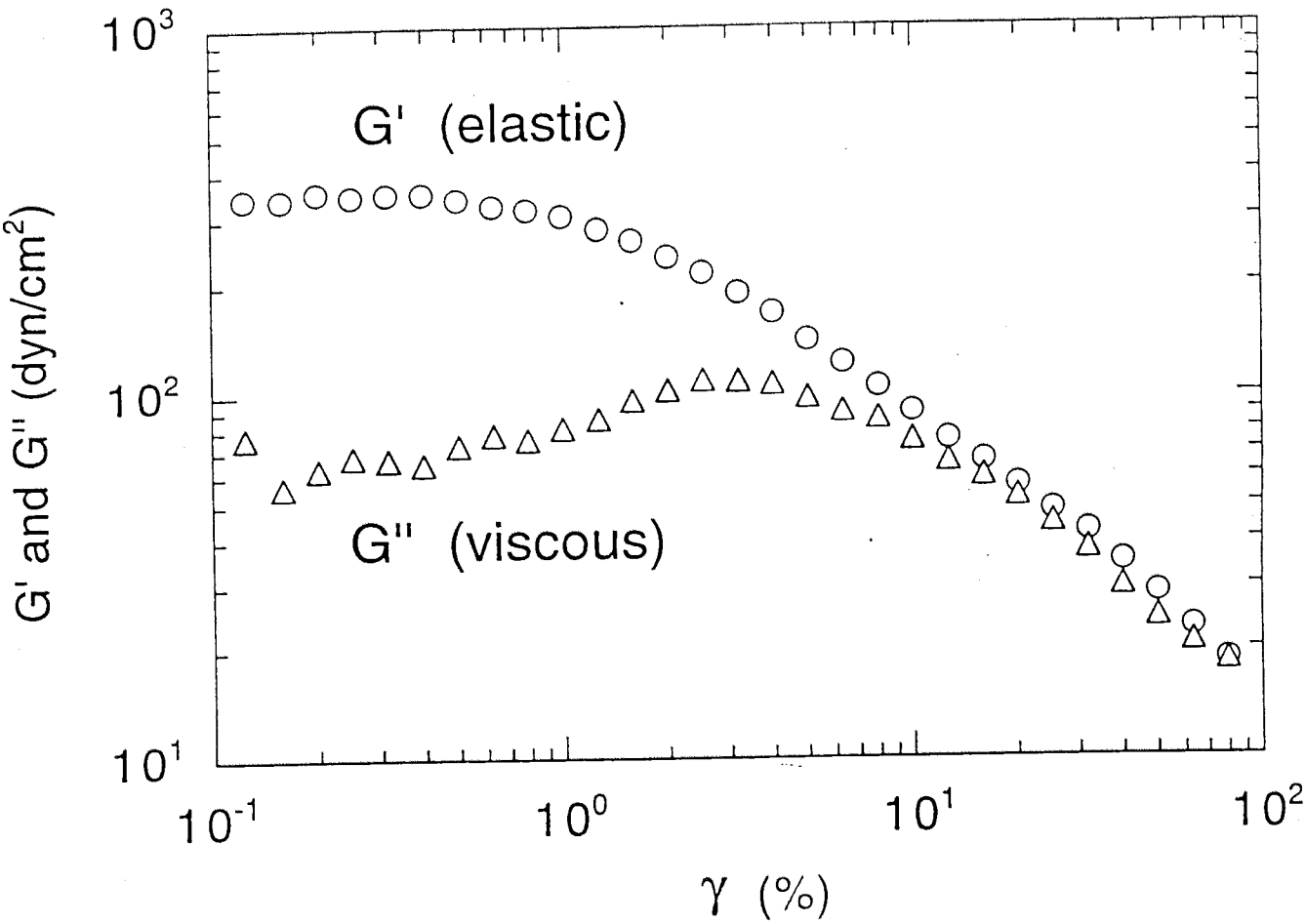

Figure 18: Dynamic moduli G' (elastic) and G" (viscous) as a function of percent strain (γ), in a typical strain sweep oscillatory strain measurement. *T. reesei* fermentation with 5% initial cellulose, 1.3 days after inoculation.

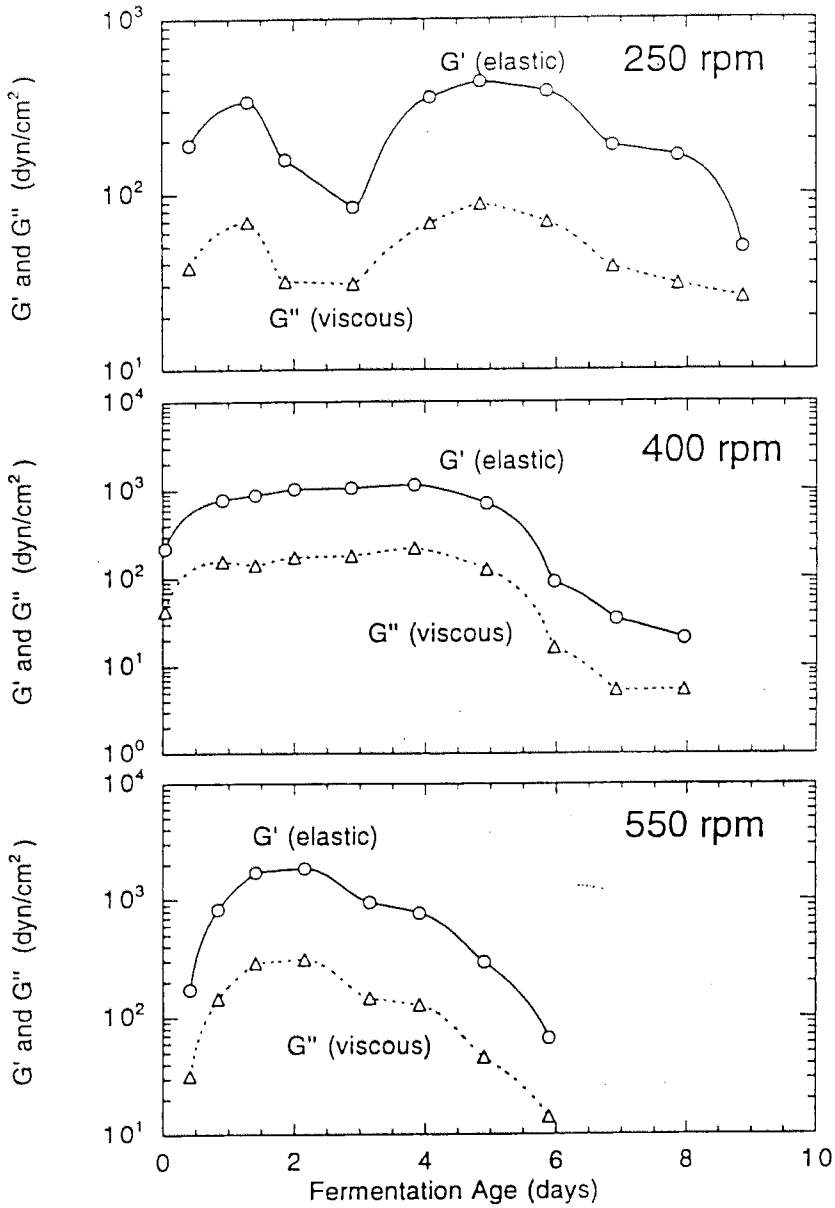

Figure 19: Average G' and G" strain sweep plateau values from three fermentations with 5% initial cellulose. Fermentor impeller speeds of 250, 400 and 550 rpm.

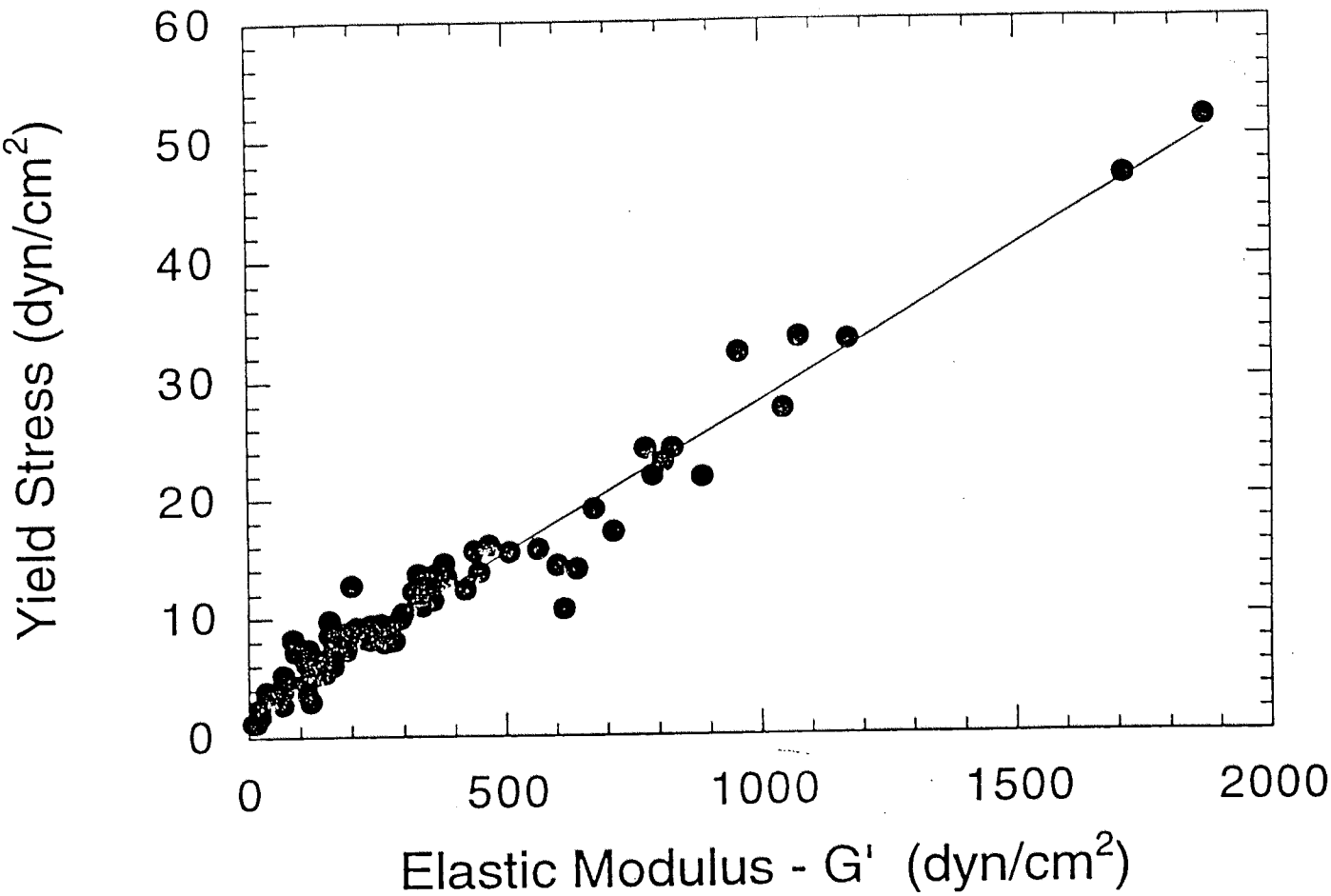

Figure 20: Correlation between yield stress and elastic modulus; line represents linear regression, $r^2 = 0.956$.

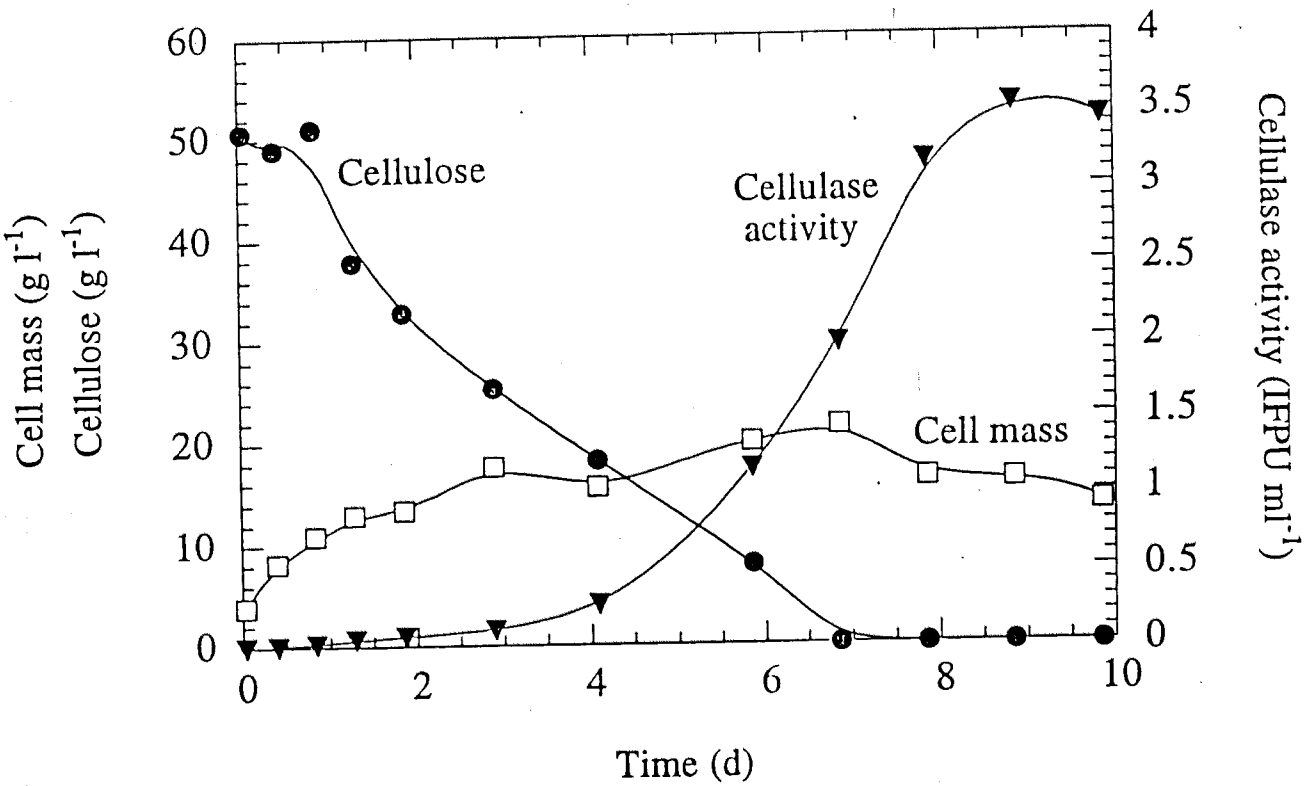

Figure 21: Cellulase production fermentation.

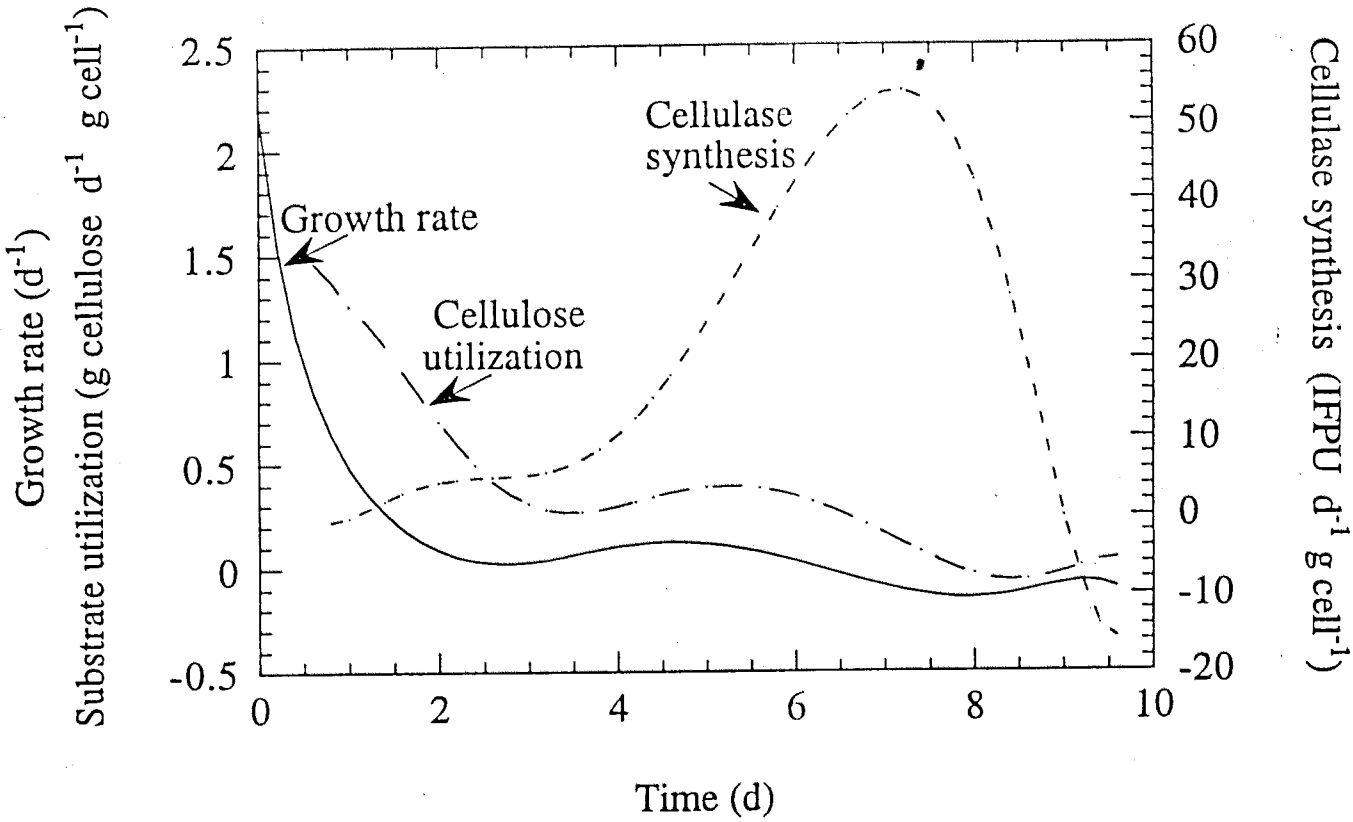

Figure 22: Cellulase production fermentation: Specific rates.

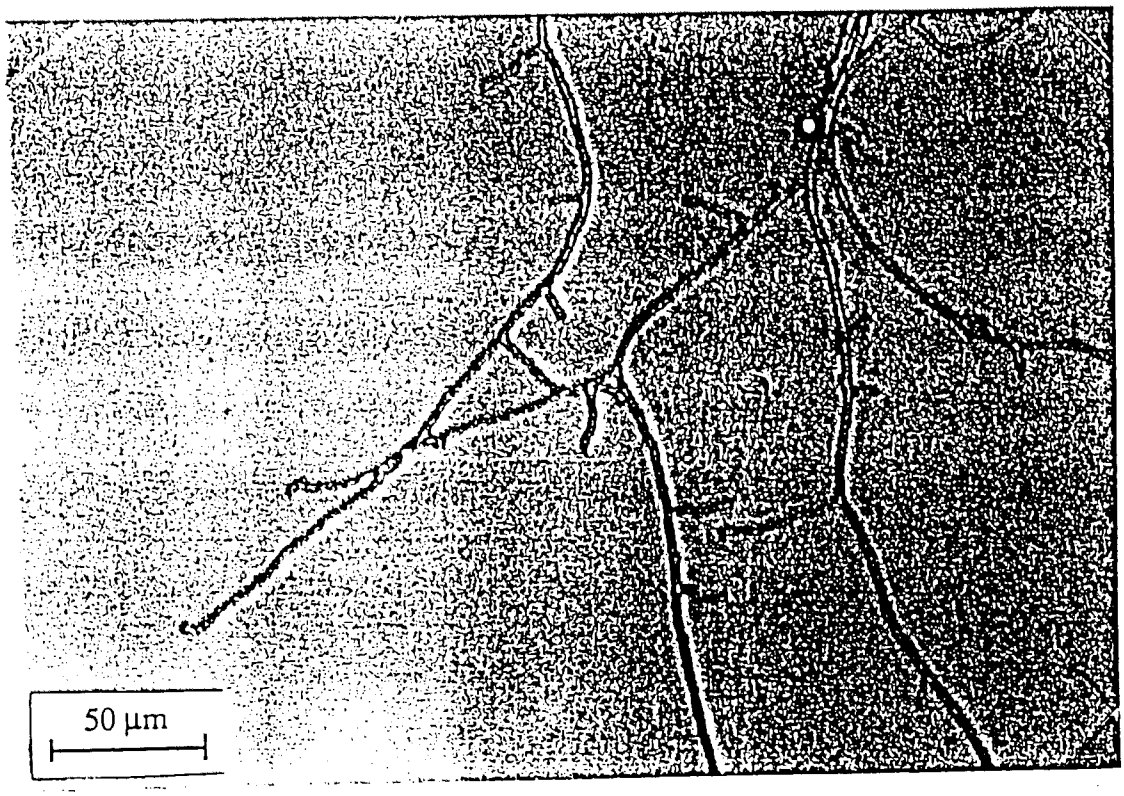

Figure 23: Primary mycelium of *Trichoderma reesei* RUT C30, 1 day old.

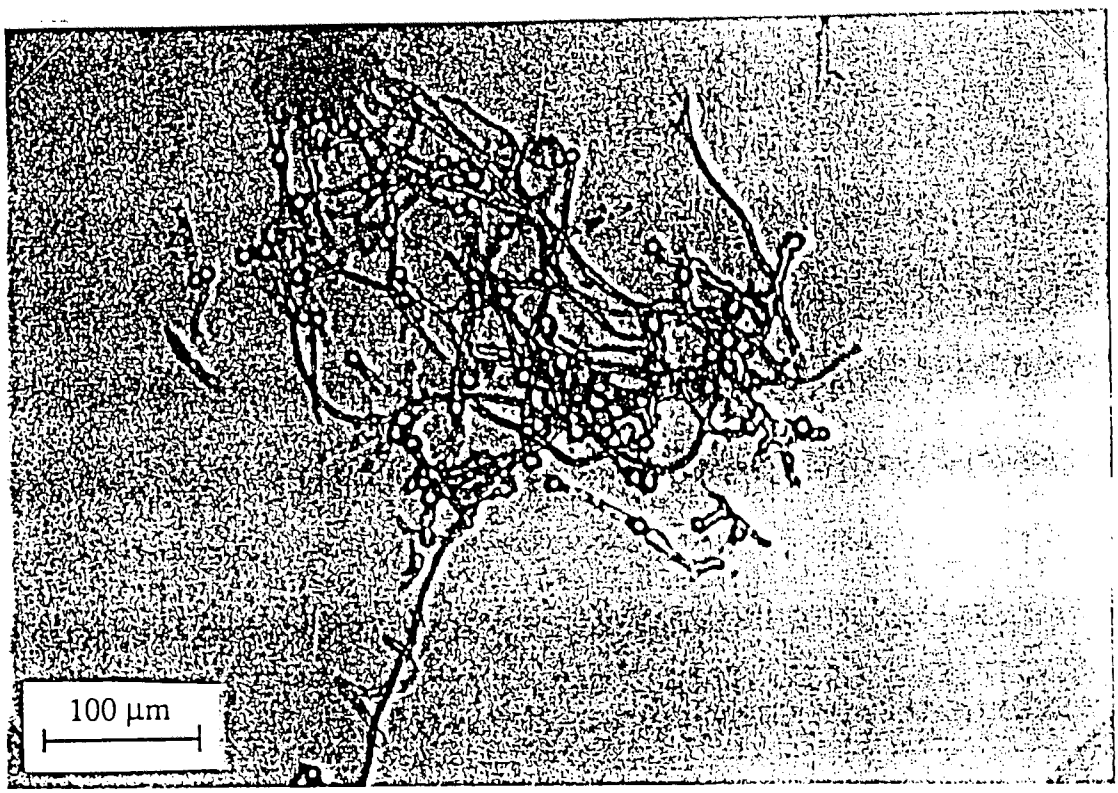

Figure 24: Secondary mycelium of *Trichoderma reesei* RUT C30, 6 day old.

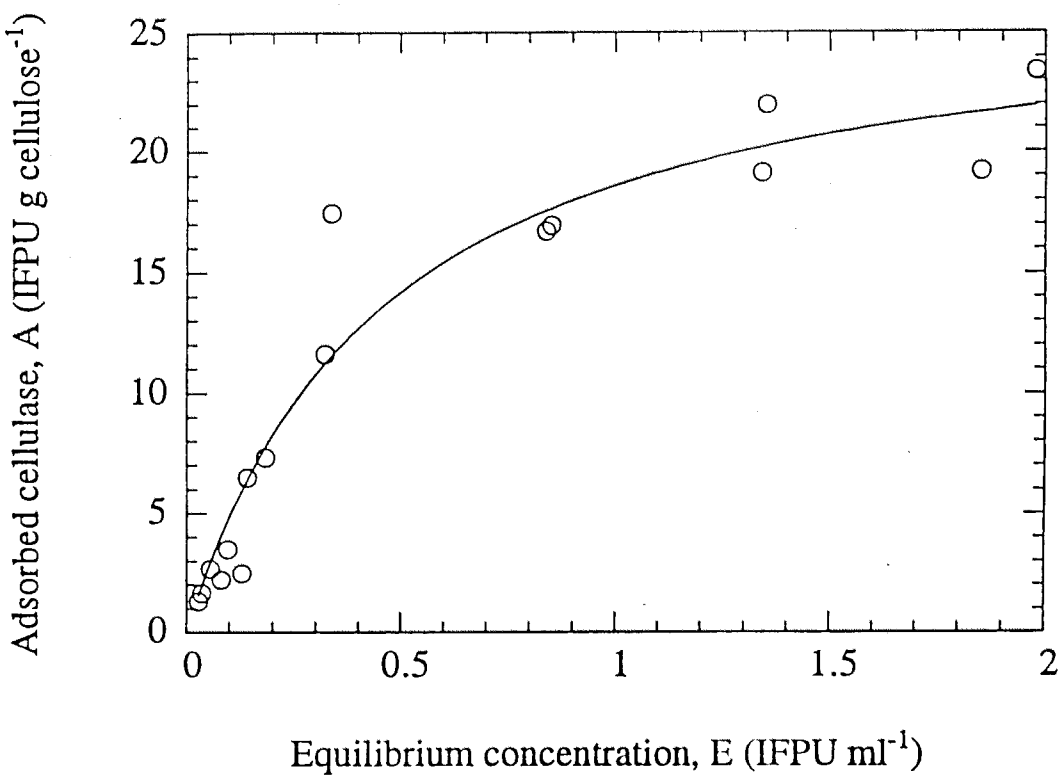

Figure 25: Adsorption isotherm of cellulases on cellulose at 28°C. Data (symbol), fitted isotherm of equation (23) (solid line).

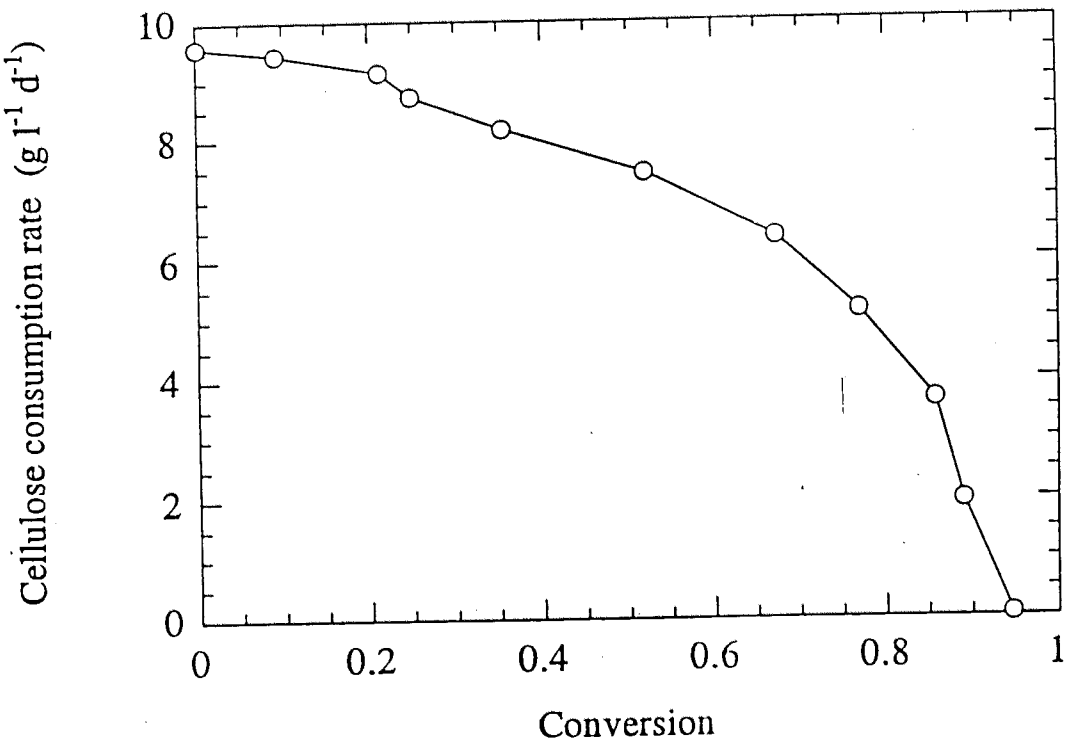

Figure 26: Cellulase fermentation: Decline of cellulose utilization rate during the course of reaction.

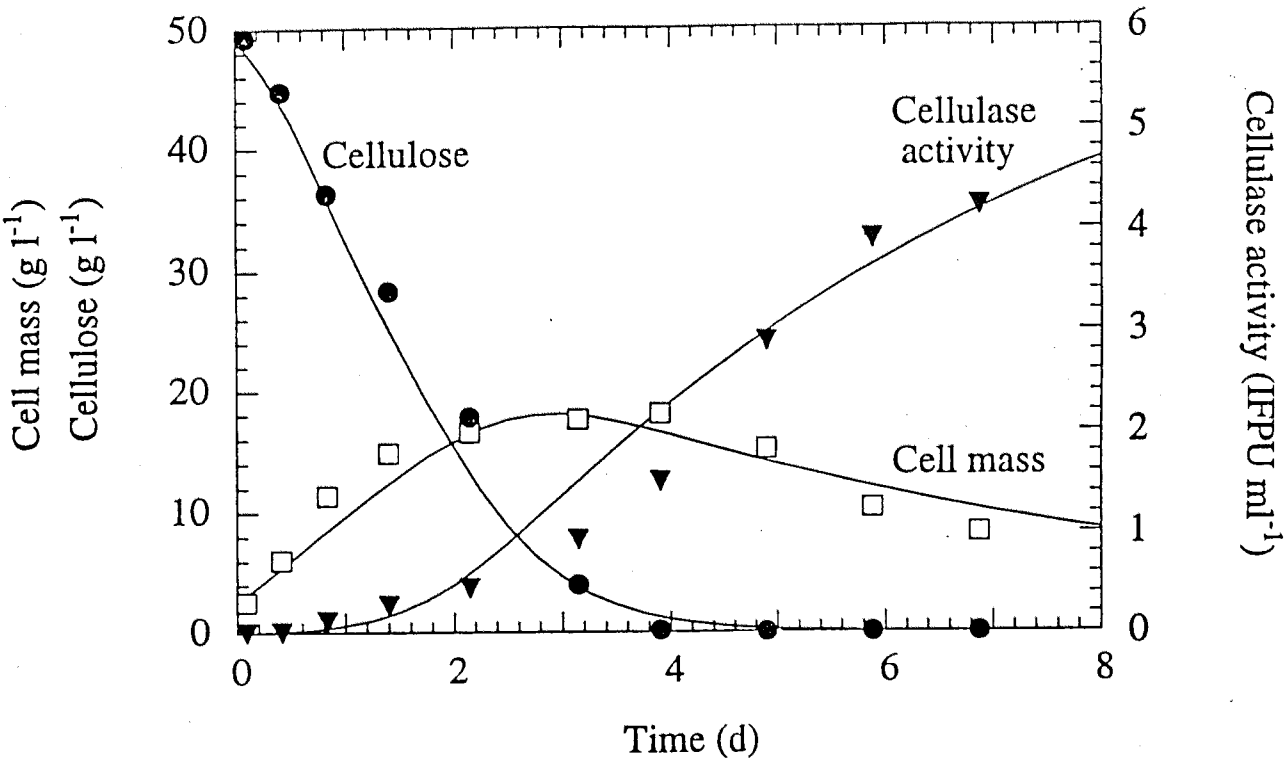

Figure 27: Cellulase production kinetics of *Trichoderma reesei* RUT C30 at 550 rpm (Run 1). Comparison of the model (solid line) and experimental data (symbols).

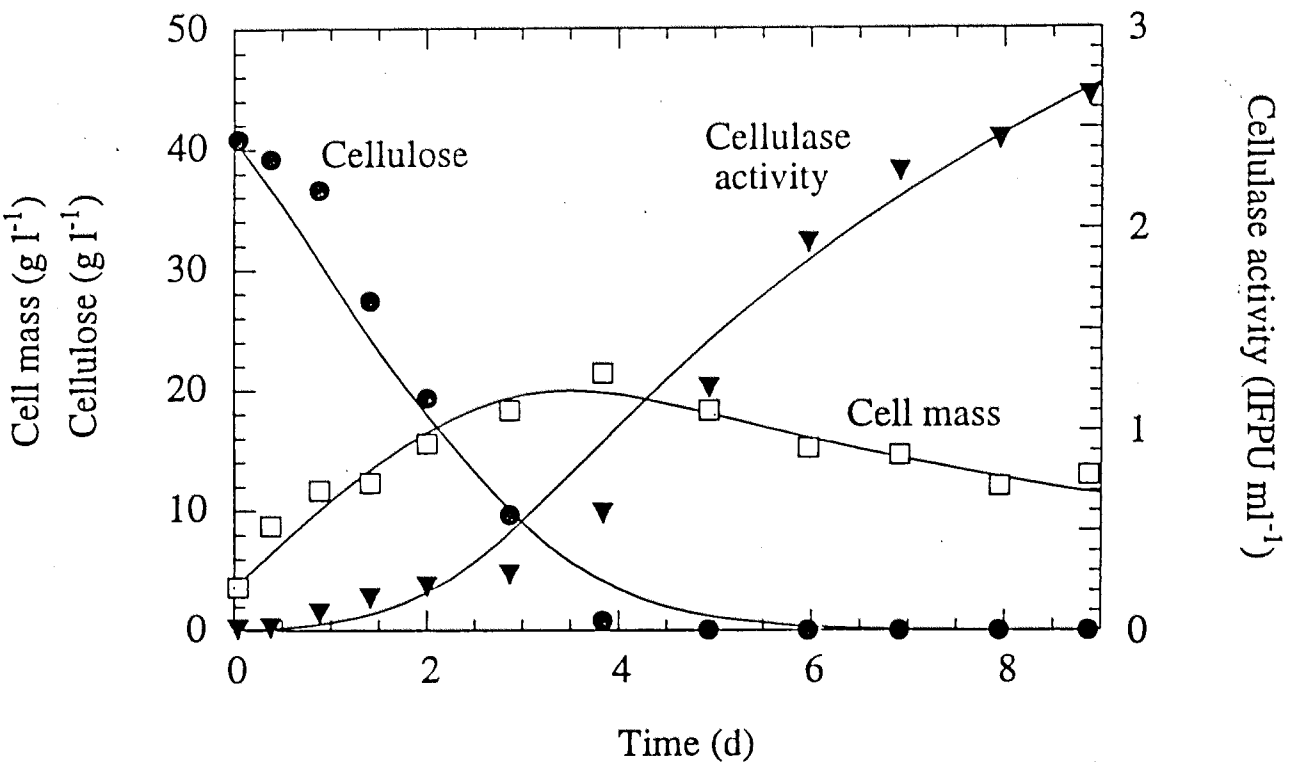

Figure 28: Cellulase production kinetics of *Trichoderma reesei* RUT C30 at 400 rpm (Run 2). Comparison of the model (solid line) and experimental data (symbols).

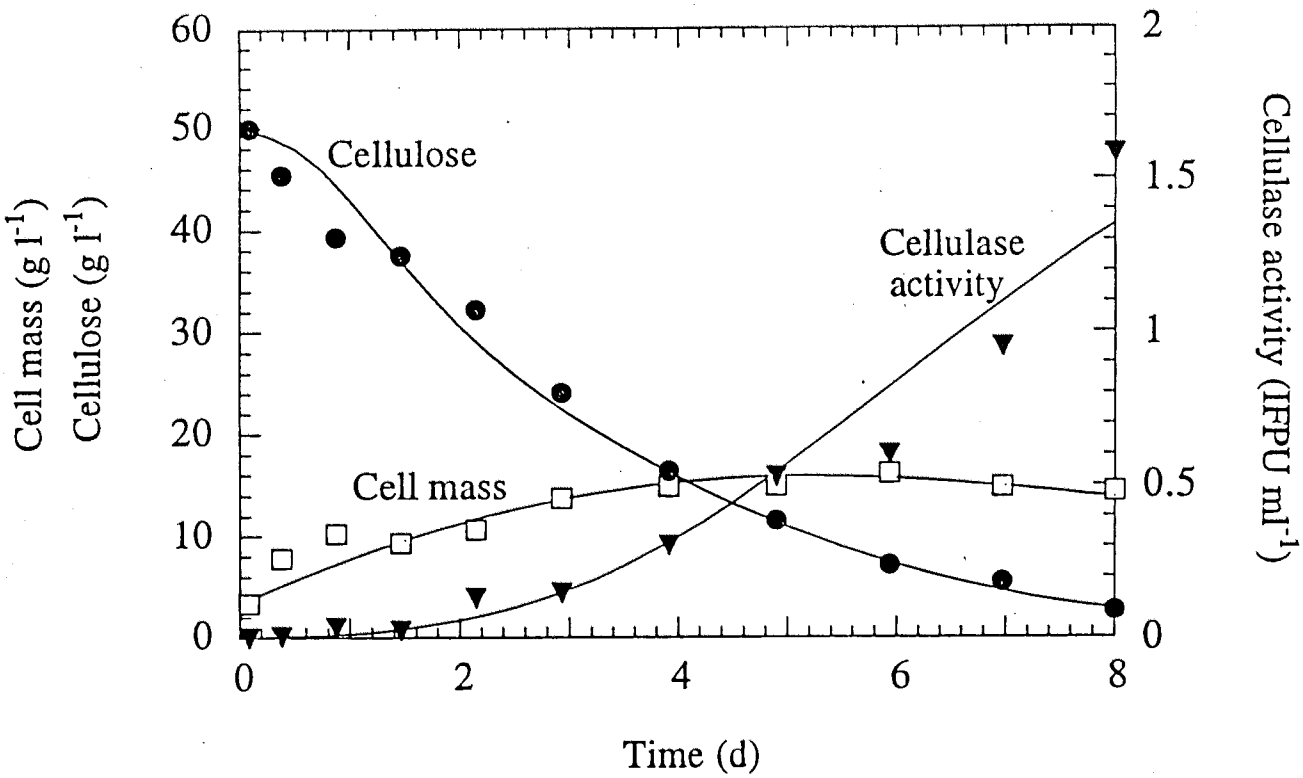

Figure 29: Cellulase production kinetics of *Trichoderma reesei* RUT C30 at 250 rpm. (Run 3). Comparison of the model (solid line) and experimental data (symbols).

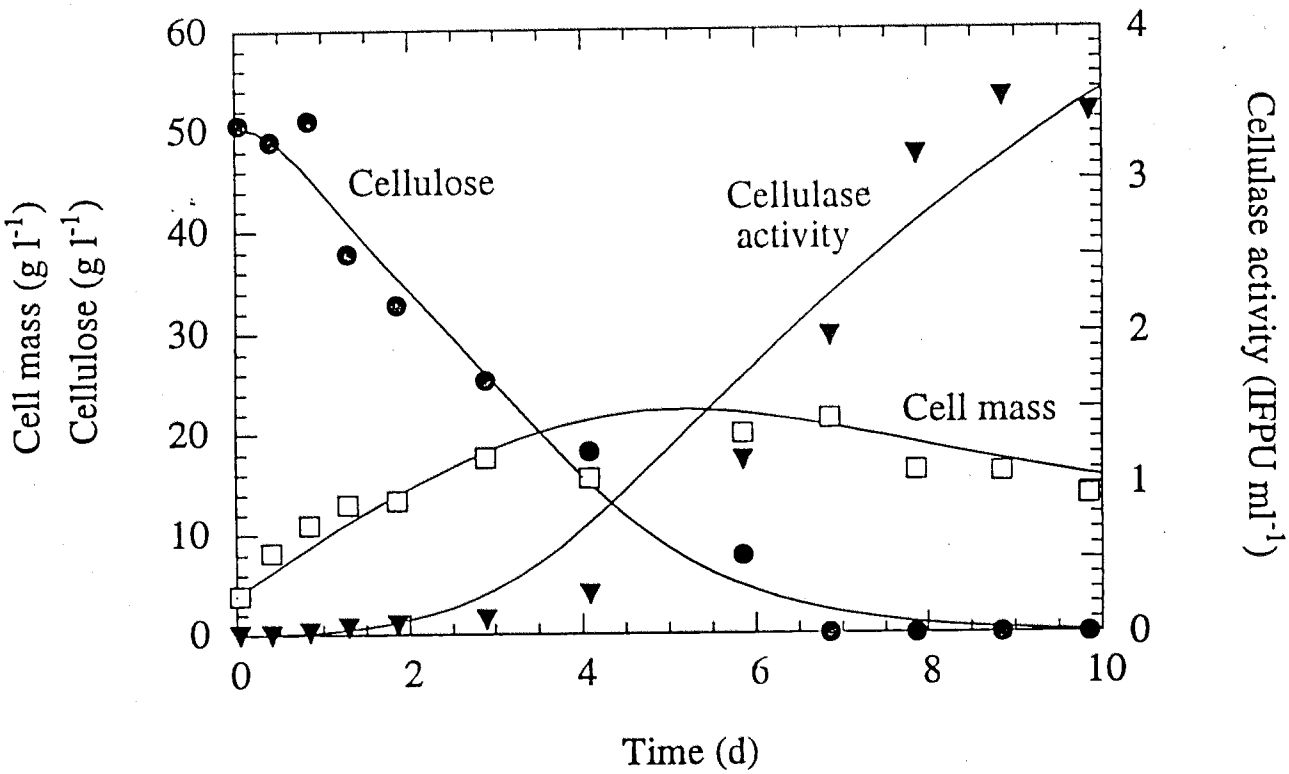

Figure 30: Cellulase production kinetics of *Trichoderma reesei* RUT C30 at 250 rpm (Run 4). Comparison of the model (solid line) and experimental data (symbols).

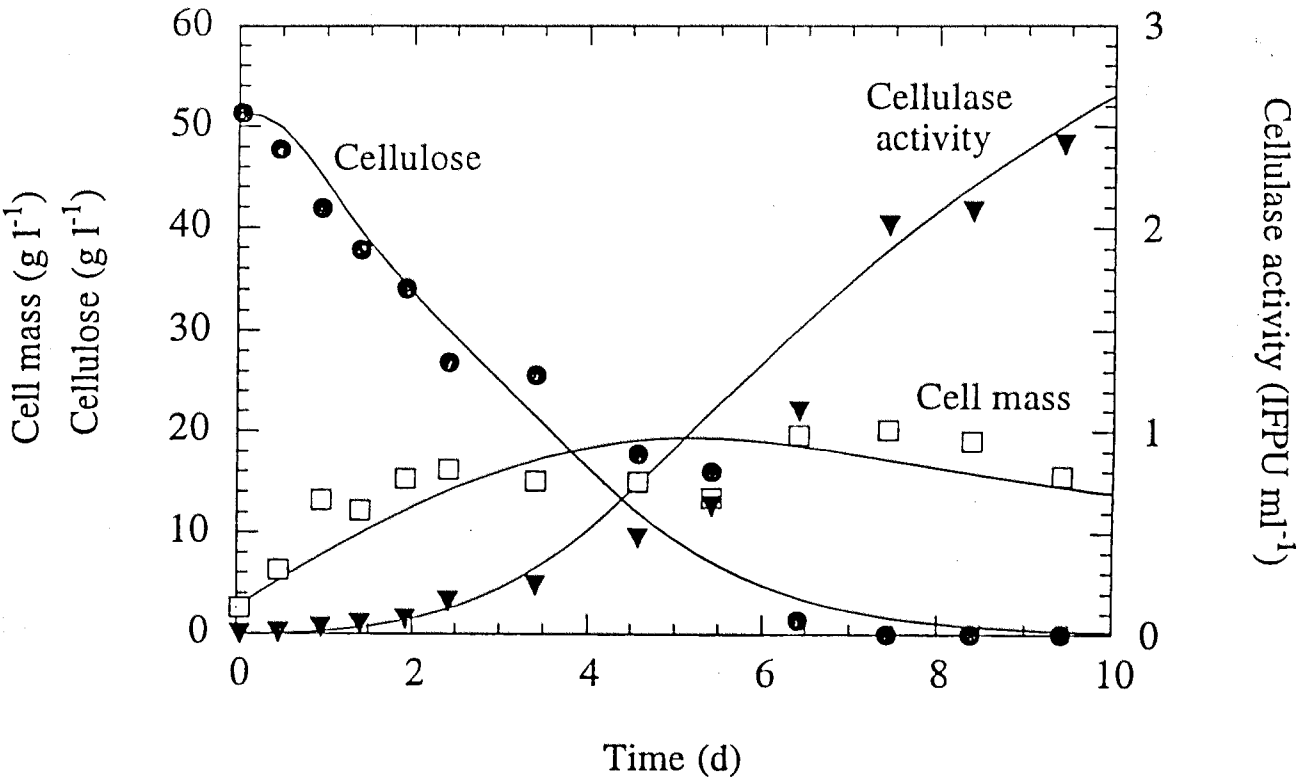

Figure 31: Cellulase production kinetics of *Trichoderma reesei* RUT C30 at 250 rpm (Run 5). Comparison of the model model (solid line) and experimental data (symbols).

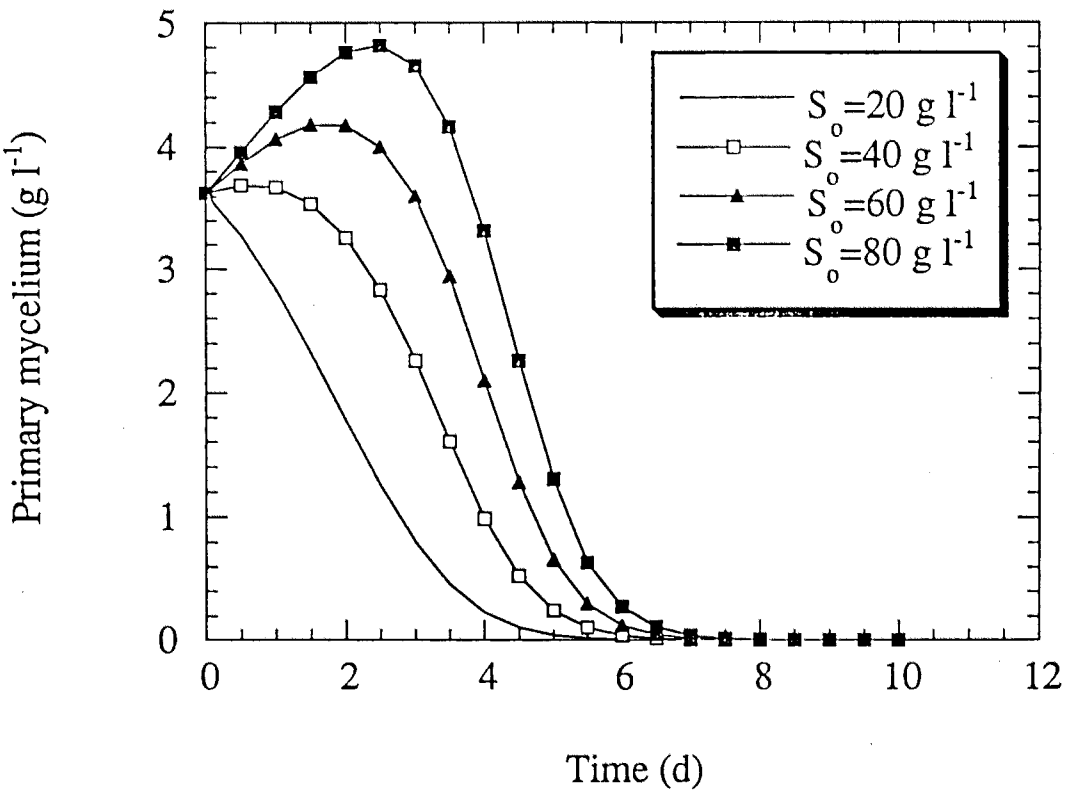

Figure 32: Primary mycelium growth curves at different initial cellulose concentrations in *Trichoderma reesei* RUT C30 fermentation.

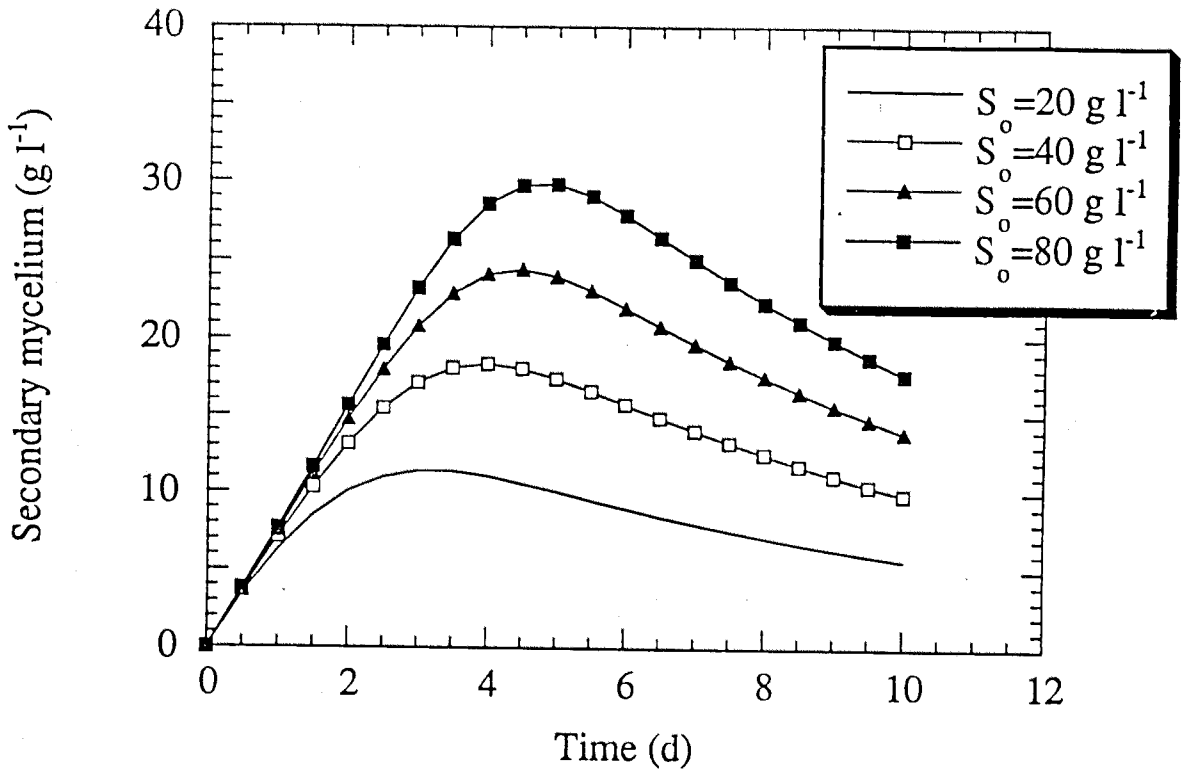

Figure 33: Secondary mycelium growth curves at different initial cellulose concentrations in *Trichoderma reesei* RUT C30 fermentation.